MEMBRANE ELECTRODE ASSEMBLY FABRICATION AND TEST METHOD DEVELOPMENT FOR A NOVEL THERMALLY REGENERATIVE FUEL CELL

by

Todd Allward

A thesis submitted to the Graduate Program in Chemical Engineering
in conformity with the requirements for
the degree of Master of Applied Science

Queen's University
Kingston, Ontario, Canada
October, 2012

Abstract

A test system for the performance analysis of a novel thermally regenerative fuel cell (TRFC) using propiophenone and hydrogen as the oxidant and fuel respectively was designed and built. The test system is capable of either hydrogen-air or hydrogen-propiophenone operation.

Membrane electrode assemblies (MEAs) were made using commercial phosphoric acid-doped polybenzimidazole (PBI) membranes and commercial electrodes. Using Pt/carbon paper electrodes with a catalyst loading of 1mg/cm^2 and a membrane with an acid doping level of 10.2 mol acid/mol of polymer repeat unit, a maximum performance of 212 mW/cm^2 at a current density of 575 mA/cm^2 was achieved for baseline hydrogen-air testing at 110°C. Problems were encountered, however, in achieving consistent, reproducible performance for in-house fabricated MEAs. Furthermore, *ex-situ* electrochemical impedance spectrometry (EIS) showed that the phosphoric acid-doped PBI was unstable in the propiophenone and that acid-leaching was occurring.

In order to have MEAs with consistent characteristics for verifying the test system performance, commercial phosphoric acid-doped PBI membrane electrode assemblies were used. At a temperature of 160°C and atmospheric pressure with hydrogen and air flowrates of 150 mL/min and 900 mL/min respectively a maximum power density of 387 mW/cm^2 at a current density of 1.1 A/cm^2 was achieved. This performance was consistent with the manufacturer's specifications and these MEAs were subsequently used to verify the performance of TRFC test system despite the EIS results that indicated that acid-leaching would probably occur.

The Pt catalyzed commercial MEAs achieved very limited performance for the hydrogenation of the ketone. However, the performance was less than but comparable to similar results previously reported in the literature by Chaurasia *et al.* [1].

For pure Pt catalyst loading of 1 mg/cm^2, using a commercial PBI MEA operating at 160°C and atmospheric pressure, the maximum power density was 40 µW/cm^2 at a current density of 1.3 mA/cm^2. A 16 hour test was conducted for these conditions with a constant 1 ohm load, successfully demonstrating the operation of the test system. The test system will be used in the development of better catalysts for ketone hydrogenation.

Acknowledgements

I want to begin by thanking my supervisors, Dr. Brant Peppley and Dr. Philip Jessop. Your guidance has been essential to the progression of my research, and your enthusiasm for your work has been inspirational. Much of my project's funding came from an NSERC strategic research grant, for which I am grateful. Thank you to the other members of the TRFC research group; Darrell, Keith, Nurul, Vanessa and Mark, it was always helpful to hear your opinions regarding my research. In particular, thank you to Vanessa Little for running gas chromatography and mass spectrometry analyses.

Thank you as well to Ela Halliop for teaching me everything I know about fuel cell hardware, assembly and operation. Your help in the laboratory was invaluable.

I must also thank the employees of Danish Power Systems®, especially Dr. Thomas Steenberg. The materials you supplied enabled me to complete my degree, but the advice and suggestions you offered helped me to understand what I was doing wrong.

Shannon, you are incredible, and I could not have done this without you. You are the most supportive person I have ever known, and I love you. Thank you to my families for all of the innumerable ways you have helped me through my time at Queen's.

Finally I must thank Izzy, whose smiling face never failed to cheer me up on gloomy days.

List of Acronyms

DL- Doping level

EIS - Electrochemical impedance spectroscopy

MEA - Membrane electrode assembly

PBI - Polybenzimidazole

RH - Relative humidity

SPEEK - Sulfonated Poly ether ether ketone

TRFC - Thermally regenerative fuel cell

GC – Gas chromatograph

Table of Contents

List of Figures

List of Tables

Chapter 1 Introduction

1.1 Waste Heat Generation and Rejection

Vast amounts of high quality waste heat are produced during energy production. This thermal energy is sometimes captured and used but is often seen as unavoidable process inefficiency and vented to available heat sinks. Figure 1 shows the United States' energy flow diagram for 2010 and illustrates the massive inefficiencies that are inherent to modern energy production.

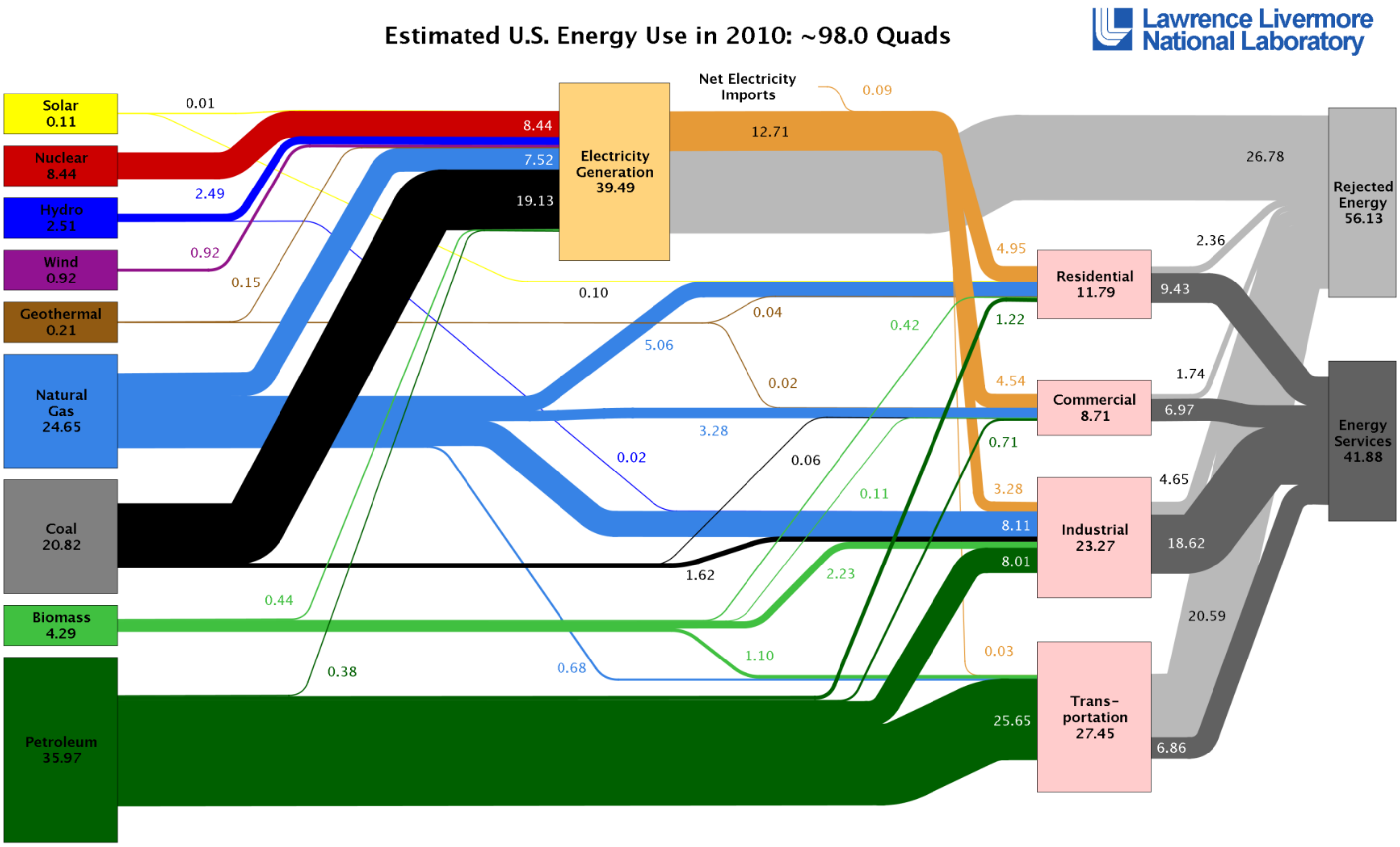

Source: LLNL 2011. Data is based on DOE/EIA-0384(2010), October 2011. If this information or a reproduction of it is used, credit must be given to the Lawrence Livermore National Laboratory and the Department of Energy, under whose auspices the work was performed. Distributed electricity represents only retail electricity sales and does not include self-generation. EIA reports flows for hydro, wind, solar and geothermal in BTU-equivalent values by assuming a typical fossil fuel plant "heat rate." (see EIA report for explanation of change to geothermal in 2010). The efficiency of electricity production is calculated as the total retail electricity delivered divided by the primary energy input into electricity generation. End use efficiency is estimated as 80% for the residential, commercial and industrial sectors, and as 25% for the transportation sector. Totals may not equal sum of components due to independent rounding. LLNL-MI-410527

Figure 1: 2010 US energy production and end uses [2]

The United States produced 98 quads (1 quad = $1.055\text{x}10^{18}$J) of energy in 2010. Of this total amount 56.13 quads (57.3% of the total) were rejected as waste heat. The energy flow diagram in Figure 1 shows that most rejected energy is generated by two sources: the electricity production and transportation industries together accounted for 84% of the total US rejected energy.

Many energy conversion processes can be made to approach efficiencies of 100% through optimization. No attempts at optimizing a continuous process for the conversion of heat into mechanical or electrical energy have succeeded, however, and conversion efficiencies have not exceeded approximately 40% [3]. Systems that absorb heat from a high temperature, produce work, and reject heat to the surroundings at a lower temperature are called heat engines. The thermal efficiency of a heat engine is dictated by the amount of heat absorbed by the system (Q_H) and the amount of heat rejected by the system (Q_C), and can be calculated using Equation 1.

$$\eta = 1 - \frac{|Q_C|}{|Q_H|} \tag{1}$$

In 1824 Carnot described the characteristics of an ideal reversibly operating heat engine. The Carnot efficiency can be calculated for non-ideal heat engines and is seen as the maximum attainable thermal efficiency of the system. Equation 2 can be used to calculate the Carnot efficiency of a heat engine. In Equation 2 T_C is the temperature of the cold reservoir and T_H is the temperature of the hot reservoir.

$$\eta_C = 1 - \frac{|T_C|}{|T_H|} \tag{2}$$

In practice large bodies of water are used industrially as cold reservoirs and have temperatures close to 300K, and combustion of fossil fuels provides the hot reservoir with a temperature of approximately 600K. The Carnot efficiency of a heat engine with these reservoirs can be calculated to be 50% using Equation 2.

There are ways, however, to compensate for the inefficiencies of the heat engine. Combined heat and power plants generate electricity in the same way as conventional power plants, but capture and use their own waste thermal energy to provide heating for buildings or other processes. Low quality waste heat can also be used to generate electricity in the Organic Rankine Cycle where organic fluids are heated past their boiling points and the vapor is used to run a turbine. Organic Rankine Cycles are useful because some organic liquids have boiling points lower than 100°C and can be used when the thermal energy source provides heat at low temperature. Found Energy is a company specializing in the application of the Organic Rankine Cycle for waste heat's capture and conversion into electricity [4]. Found Energy's Rosetown Waste Heat Recovery project at the TransGas Rosetown Compressor Station in Saskatchewan captures waste heat from a gas turbine's engine exhaust and generates approximately 7,000,000 kWh per year. The electricity produced from waste heat at this station provides sufficient energy to power 800 Saskatchewan homes.

1.2 Fuel Cells

Fuel cells are electrochemical systems that liberate the chemical energy of a fuel to produce electricity. Unlike heat engines fuel cells do not ignite and burn fuel and are consequently not limited by the Carnot efficiency that governs the ideal efficiency of a heat engine. Many conventional fuel cells use hydrogen as a fuel, oxygen or air as an oxidant, and yield water as a product. Fuel cells are consequently regarded as being a green technology. Figure 2 shows the basic operation of a conventional fuel cell run on hydrogen and air.

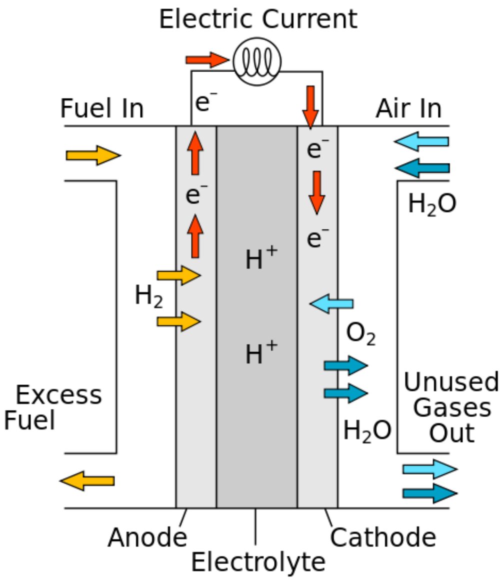

Figure 2: Schematic diagram of a generic hydrogen-oxygen fuel cell [5]

The current produced by a fuel cell is directly proportional to the rate of the catalyzed reactions occurring on the electrodes [6]. These rates are themselves proportional to the amount of catalyst available for reaction. Modern catalysts have porous microstructures that provide effective surface areas many thousands of times their actual surface area. These higher effective surface areas expose more catalyst particles to reactant gases at any given time and consequently permit a higher rate of electron flow through the circuit. Fuel cell performance is therefore often reported on a per area basis so that results can be normalized across differently-sized electrode areas.

1.3 Direct Conversion of Heat to Electricity

1.3.1 Thermoelectric Devices

Thermoelectric (TE) devices are compact solid-state semiconductor-based systems that are able to convert between thermal and electric energy [7]. The thermoelectric phenomenon was first noted in 1823 by Thomas Seebeck when he observed a voltage drop across a sample exposed to a temperature gradient. Figure 3 shows a system illustrating the Seebeck effect.

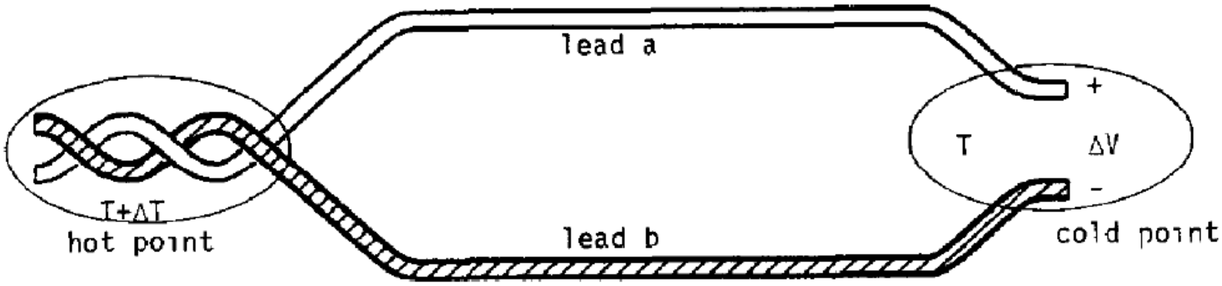

Figure 3: Semiconductor system demonstrating the Seebeck Effect [8]

Seebeck discovered that if two semiconductors were joined at a hot point and their terminals were kept at a lower temperature a potential difference developed between the terminals at the cold point; when the terminals were joined at the cold point a current was observed flowing through the completed circuit. TE devices have no moving parts and are therefore quite rugged and durable but are limited by their low efficiencies, which are approximately 10% of their Carnot efficiency. Thermoelectric devices are consequently often used where efficiency is of less importance than the relative size or reliability of the device [9].

1.3.2 Thermally Regenerative Fuel Cells

In a regenerative fuel cell system, fuel and oxidant are converted back into an energy storage chemical that can be used repeatedly in the generation of electricity [10]. Thermally regenerative fuel cells (TRFCs) can, therefore, be seen as an energy storage system that as a process has thermal energy as an input and electrical energy as an output. Regenerative electrochemical systems can use a variety of energy sources (electrical, photovoltaic, thermal, etc.) to regenerate their working substance, but the TRFC is designed around the use of heat as an energy source.

1.4 Historical Thermally Regenerative Fuel Cell Research

Liebhafsky [11] considered nuclear energy to be a potentially useful source of waste heat for a TRFC, likely due to the abundance of available nuclear energy at the time and the quality of the heat that it provided. Although a conventional fuel cell is not limited by the Carnot efficiency because it does not convert heat directly into electricity, the TRFC's combination of heat source and fuel cell will have a maximum ideal efficiency defined by Carnot's theorem.

TRFC research has been broadly focused, and the different systems that have been proposed are related only through the general definition of a TRFC. Studied systems have included thermally regenerative gas-phase concentration cells [12] and thermally regenerative liquid metal cells using mixtures of Na/Hg [13][14], Na/Sn [15], and K/Hg,

Research in Japan has extensively studied low temperature organic liquid-based TRFC systems. A TRFC was proposed in which 2-propanol was dehydrogenated by solar energy to yield acetone and hydrogen [16]. A number of papers related to the subject were published over the subsequent decade focusing on the optimization of catalyst systems.

1.5 Concurrent Thermally Regenerative Fuel Cell Research

TRFC research at Queen's University has been ongoing for several years. The proposed experimental system was developed and based on this previous research. Figure 4 shows a simplified schematic of the proposed system.

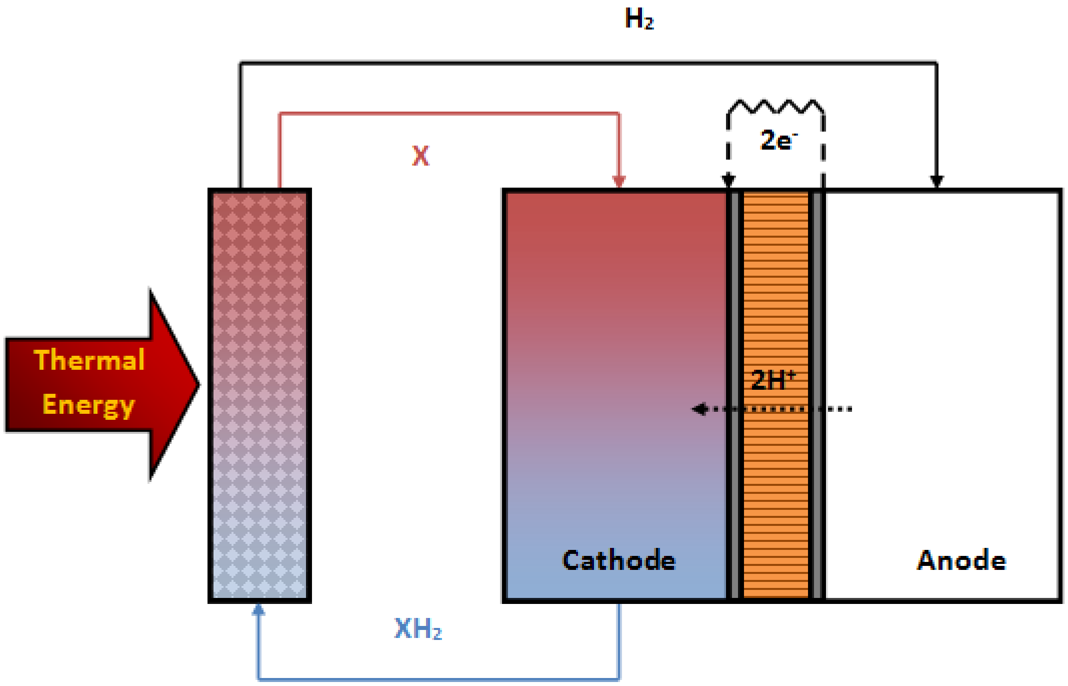

Figure 4: Simplified schematic of proposed TRFC system

In the proposed system a liquid working substance XH_2 is dehydrogenated in an external catalyzed reaction using thermal energy. Hydrogen gas is fed to the anode of the fuel cell where it is oxidized to produce protons and electrons. Protons pass through the membrane to the cathode, and electrons pass through an external circuit to produce useful electricity. At the cathode liquid substance X, the electrons and the protons are combined to regenerate working substance XH_2, and the cycle is repeated.

Concurrent research by Carrier determined a suitable working substance pair (X and XH_2) for the TRFC system [17]. The suitability of the working substances was determined by the selectivity and reversibility of the hydrogenation and dehydrogenation reactions, and the toxicity and thermal stability of the two substances. Reaction selectivity is important in the proposed TRFC because of system's cyclic nature. Reaction by-products will build up and decrease the total amount of working substance available to the system, and if the hydrogenation is not reversible the cyclic nature of the system is not possible. Propiophenone and 1-phenyl-1-propanol were chosen as working substances X and XH_2 respectively. The selected compounds and the related hydrogenation and dehydrogenation reactions are shown in Figure 5.

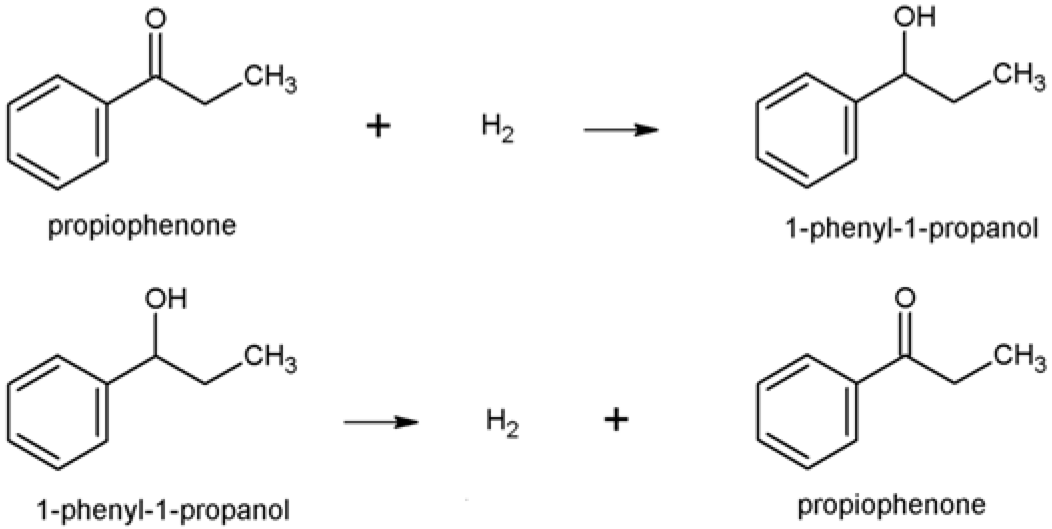

Figure 5: Selected working fluid pair and associated hydrogenation/dehydrogenation reactions for the proposed TRFC system

Separate concurrent research by Dean examined potential catalyst systems for the hydrogenation of propiophenone [18]. An ideal catalyst system would enable a high rate of reaction while maintaining extreme reaction selectivity with respect to the desired hydrogenation. The rates of reaction of platinum and palladium catalyst were comparable, however, it was found that the best selectivity was obtained with palladium catalysts, leading to Dean's recommendation that further optimization be done on palladium-based catalyst systems in order to increase both the rate and selectivity. It was observed that suitable hydrogenation reaction rates were only obtained at temperatures above 100°C.

1.6 Benefits of the Proposed Thermally Regenerative Fuel Cell

It is proposed that this TRFC could be used as part of the radiator system of a long-haul transport truck. The external dehydrogenation reactor could use waste heat from the radiator, providing additional cooling for the engine block and waste heat to run the TRFC. Implementation of the proposed system would increase fuel efficiency of the truck by producing supplementary electricity without additional fuel consumption.

A truck's alternator scavenges a small amount of mechanical energy from the engine and converts it into electrical energy that is used to run the auxiliary systems. The energy used by the alternator decreases the total amount of energy from the fuel that goes into powering the drive train and consequently decreases the fuel economy of the vehicle. For a standard transport tractor increases in alternator efficiency from 50% to 60% would result in fuel savings of 250 USD per year [19]. An optimistic outlook on the current research is that a TRFC could completely replace the alternator, potentially saving upwards of a thousand dollars a year in wasted fuel per vehicle. With 11 million medium and heavy trucks on US road alone in 2008, and 684,000 new trucks added that year alone, there are substantial economic incentives to increase the fuel economy of the transportation industry [20].

1.7 Project Objectives

The objectives of this project are: 1) to design and build a test system for the performance evaluation of the proposed TRFC. This test system will be used in the current experimental work as well as by future researchers involved in the TRFC project. 2) To locate a fuel cell membrane that will function in the high temperature organic liquid environment of the TRFC. While a review of current commercially available membranes will be used to make an initial selection, experimental testing will conclusively judge material compatibility. 3) To obtain initial estimates of the TRFC performance of a fuel cell using the previously selected membrane. MEAs will be fabricated inhouse and their performance will be compared to that of commercial MEAs. The baseline hydrogen-air performance of the MEAs will be used to determine their quality. MEAs with suitably high performance will be performance tested as TRFCs.

Chapter 2 Literature Review and Theory

2.1 Thermally Regenerative Fuel Cells

Past research on thermally regenerative electrochemical cells has studied diverse systems. A continuous gas concentration cell has been studied in which iodine vapor was expanded through a PbI_2 electrolyte to generate electricity in a concentration cell [12]. It was proposed that iodine could be condensed at a cold reservoir after passing through the electrolyte and be pumped back to the pressurized high temperature side of the cell. The experimental apparatus that was used simply switched the hot and cold sides of the cell after each cycle was completed to regenerate the working substance and draw a current in the reverse direction. Very small amounts of current were drawn from the cell and the resistance of the electrolyte was found to increase over time. Further work studied the use of Na/NaCl and K/KCl concentration cells [12].

A thermally regenerative sodium-mercury galvanic system known as the thermally regenerative alloy cell (TRAC) has been studied [21]. The TRAC system used a ceramic matrix to contain an electrolyte comprised of a ternary mixture of sodium salts, and used sodium cations as the charge carrying species. A sodium-rich amalgam was oxidized to produce sodium cations at the anode. After passing through the electrolyte cations were reduced at the cathode and combined with a stream of mercury. Both the anode and cathode effluent streams contained sodium-poor amalgams. Initial research did not consider the thermally regenerative aspects of the cell but focused on determination of cell resistance and electrode polarization at various temperatures and electrode configurations.

Further research developed the regeneration system of the TRAC [13]. In the regeneration system the anode and cathode effluent amalgam streams were heated in a boiler to produce a nearly pure mercury vapor and a liquid phase of sodium-rich amalgam. The liquid and vapor phases were separated and cooled to the cell temperature, mercury was condensed, and both streams were again sent through the cell to repeat the process. Simulations of the TRAC system which were presented in a later paper estimated that the system could produce a specific power of 10 W/lb from a nuclear heat source at 7% efficiency [14].

Other metal alloys have been proposed for use in liquid-metal thermally regenerative concentration cells. Agruss *et al.* [15] proposed sodium/tin, sodium/mercury and potassium/mercury as potential alloys. Potassium/mercury alloys were examined most rigorously due to their favourable separation kinetics and because their regeneration temperature would be similar to the heat output of existing nuclear reactors. The operational principles of this cell are the same as those described earlier for the TRAC system. The research culminated in the operation of cells with power densities of up to 100 mW/cm^2.

The United States Office of Naval Research commissioned a study on TRFCs [22]. The resulting anionic membrane fuel cell produced electrons at the anode by oxidizing an ionic salt in the presence of hydrogen gas and chloride ions. The reduction of hydrochloric acid at the cathode produced chloride ions that passed through the membrane and hydrogen gas that was passed to the anode through an external circuit. Thermal distillation regenerated the ionic salt and the hydrochloric acid, which were passed back to the anode and cathode respectively. Low conductivity of the membrane and the difficult separation of hydrogen chloride gas from hydrogen gas proved problematic. A maximum power density of 0.69 mW/cm^2 was achieved.

The feasibility of running a hydrogen-oxygen fuel cell as a thermally regenerative system has been examined as an alternative to the more technologically complex thermochemical regeneration used in many TRFCs [23]. Two different regeneration methods were proposed.

The first used purely thermal energy at 2000K, and the second used a high temperature electrolysis method running at 1300K.

2.1.1 Chemical Hydrogenation/Dehydrogenation-Based Thermally Regenerative Fuel Cell Systems

A catalyst-assisted chemical heat pump was suggested by Saito *et al.* as an inexpensive way to upgrade low quality solar heat [24]. In the proposed system solar energy was used to dehydrogenate 2-propanol in an endothermic reaction, and upgraded heat was produced by the exothermic hydrogenation of acetone. Acetone and 2-propanol were selected because of their chemical stability, the selectivity of their hydrogenation/dehydrogenation reactions, and the ability of the hydrogenation reaction to utilize the low temperature heat provided by solar energy [25].

Saito *et al.*'s early work was used as the foundation for later work by Ando *et al.* on chemical hydrogenation/dehydrogenation-based thermally regenerative fuel cells using Nafion membranes [16]. In Ando *et al.*'s proposed system 2-propanol was dehydrogenated at the fuel cell anode to produce hydrogen and acetone. The hydrogen was oxidized to produce a proton that travelled through a membrane electrolyte while the electrons created a current in an external circuit and generated useful electrical power. The electrodes of the fuel cell were held at different temperatures to facilitate the reactions and to create a difference in Gibb's free energy of reaction that could be exploited to produce electricity. Acetone was removed from the anode and sent to the cathode through external tubing. At the cathode the acetone was once again hydrogenated to return 2-propanol. To evaluate the performance of the system hydrogen and acetone were passed to the anode and cathode respectively and the dehydrogenation reaction was not considered. Ando *et al.* examined different catalysts and found that a mixed platinum/ruthenium (Pt/Ru) catalyst system yielded superior performance than either monometallic catalyst system with respect to both reaction conversion and rate. At 90°C Ando *et al.* observed an open circuit voltage between 110-120 mV and a short-circuit current density of 2.4 mA/cm^2 when using a Pt/Ru catalyst loading of 3 wt%.

The performance of the acetone/2-propanol TRFC system was later analyzed using a variety of Pt/Ru catalyst loadings [26]. The TRFCs were operated at 60°C with hydrogen and dilute acetone flow to the anode and cathode respectively and a fuel utilization of 0.6% at the short circuit current density. A maximum power density of 175 µW/cm2 was achieved using a large catalyst loading of 30 wt% as presented in Table 1.

Table 1: Reported Gas-Phase TRFC Performance for Various Catalyst Loadings [26]

Catalyst Loading	Approximate Maximum Power Density (µW/cm^2)
3 wt% (19.5 mg/cm^2)	50
5 wt% (41 mg/cm^2)	56
30 wt%	175

In a further experiment, Ando *et al.* attempted to dehydrogenate dilute 2-propanol directly at the anode and hydrogenate acetone at the cathode in what they referred to as a liquid-phase TRFC [26]. Their best performing liquid phase TRFC produced a power density of approximately 6.9 µW/cm^2 with an open circuit voltage of approximately 18 mV. The cell was operated at 60°C with dilute 2-propanol and acetone flow and a fuel utilization of 0.09% at the short circuit current density. The catalyst loading was reported as 50 wt%.

In subsequent work by Ando and Tanaka, polarization plots were developed for Nafion membrane TRFCs running at 60°C using membranes of varying thickness [27]. To simulate a practical system a mixture of equal parts acetone and 2-propanol was fed to the cathode after being diluted tenfold with water to maintain electrolyte conductivity, and hydrogen was fed to the anode. A maximum current density was produced when using Nafion® N115 membranes. Cells using Nafion® N115 membranes produced current densities 20% larger than cells using Nafion® N112 or Nafion® N1135 membranes and 50% larger than cells with Nafion® N117 membranes. It was proposed that the 127 µm thickness of Nafion® N115 membranes optimized hydrogen crossover and membrane ohmic resistance. With a total Pt/Ru catalyst loading of 30 wt% a short circuit current density of approximately 29 mA/cm^2 and open circuit voltages of approximately 100 mV were reported along with an apparent maximum power density of approximately 0.63 mW/cm^2.

Choosing to optimize the better performing TRFC system, Ando *et al.* turned their focus to the study of the gas phase TRFC [28]. Using a ruthenium/platinum catalyst loading of 30 wt% it was found that the cathode temperature strongly influenced the performance of the TRFC and that an increase in temperature from 50°C to 60°C raised the short circuit current density from approximately 6 to 10 mA/cm^2. Ando *et al.* also studied the effect of fuel cell compression on the performance of the gas phase TRFC. Additional sheets of carbon cloth were added to either side of the membrane electrode assembly to increase the contact of the electrolyte and membrane. As the number of sheets of carbon cloth increased, the electrolyte was pressed against the electrode more strongly, and fuel cell performance was found to increase. The short circuit current density of the cell increased from approximately 5 mA/cm^2 up to approximately 20 mA/cm^2 with 1 and 4 additional carbon cloth sheets added respectively.

Further research by Chaurasia *et al.* [1][29] lowered the catalyst loading in their MEAs and used various Pt/Ru combinations to optimize the performance of the gas phase TRFC. It was found that Pt-based catalysts did not effectively promote the hydrogenation reaction, and the measured performance of Pt catalyst electrodes was 30% of that of the Pt/Ru composite catalyst electrodes for the same catalyst loading. The optimized total Pt/Ru catalyst loading of 5.0wt% at the anode and 7.5 wt% at the cathode produced a short circuit current density of approximately 12.5 mA/cm^2 and a maximum power density of approximately 255 µW/cm^2. A polarization curve showing this performance is given in Figure 6.

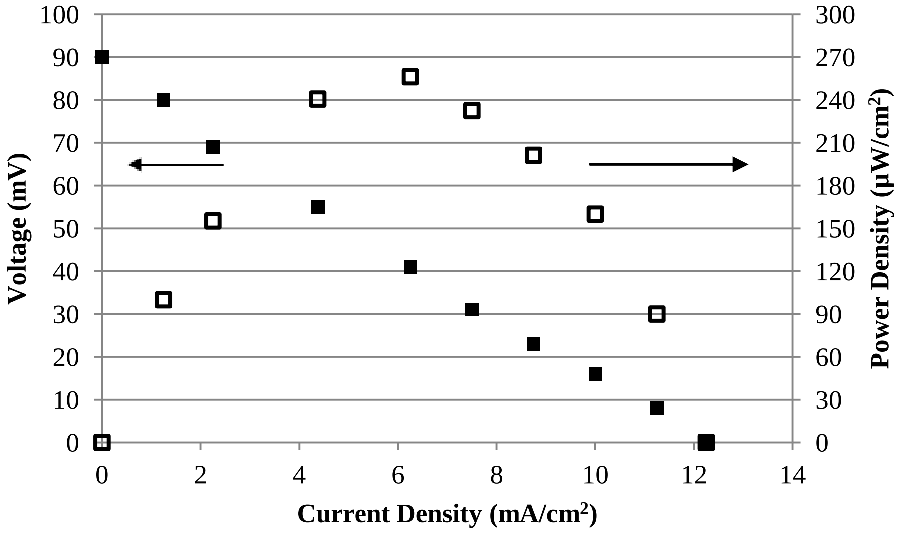

Figure 6: Polarization curve for TRFC of Chaurasasia *et al.* [29] Cell was operated at 50°C with an anodic hydrogen flow rate of 100 mL/min and a dilute acetone/2-propanol mixture cathode flowrate of 1 mL/min.

2.2 Thermodynamics of Thermally Regenerative Fuel Cells

Because the input to the TRFC is heat and the output is electricity, the system's maximum theoretical efficiency will be limited to the Carnot efficiency [30]. The maximum work of a TRFC is determined by the Gibb's free energies of the dehydrogenation and hydrogenation reactions as shown in Equation 3 [11].

$$Work = \Delta G_{hydrogenation,T_1} - \Delta G_{hydrogenation,T_2} \tag{3}$$

Assuming that the change in enthalpy of reaction and entropy of reaction with respect to temperature is negligible, Equation 3 can be simplified, yielding Equation 4.

$$Work = \Delta S_{hydrogenation} * (T_2 - T_1) \tag{4}$$

For a given pair of compounds the available work can be modified by changing the temperature of either the hydrogenation or dehydrogenation reaction. The available work is therefore dependent on the product of entropy and temperature for each reaction.

2.3 High Temperature Polymer Electrolyte Membrane Fuel Cells

High temperature polymer electrolyte membrane fuel cells have received a great deal of attention due to their simplified water management requirements, and increased reaction kinetics and carbon monoxide and sulfur tolerance with respect to PEM fuel cells. Poly ether ether ketone (PEEK) and polybenzimidazole (PBI) are two polymers that are frequently studied for use in high temperature PEM fuel cells.

Poly Ether Ether Ketone

PEEK is a highly crystalline aromatic polymer with excellent thermal and chemical stability [31]. Though its high durability is desirable for high temperature PEM fuel cell applications PEEK has very low conductivity. For use in fuel cells PEEK is typically boiled in sulfuric acid to yield sulfonated poly ether ether ketone (SPEEK) [32]. An increase in the level of sulfonation disrupts the crystallinity of the polymer, leading to increased solubility [33]. While PEEK is only soluble in some concentrated acids, SPEEK is soluble in methanol and even water at 0°C if the degree of sulfonation is high enough [32][34]. SPEEK's conductivity is due to networks of sulfonic acid groups that entrap water molecules and provide a path along which solvated protons can migrate through the membrane; SPEEK membranes are therefore only conductive when they are adequately humidified.

Polybenzimidazole

PBI is an aromatic, chemically resistant polymer that has found use as the electrolyte in high temperature polymer electrolyte membrane fuel cells. PBI is a durable polymer that, in its untreated state, has very low conductivity and is unsuitable for fuel cell membrane use. PBI's conductivity can be increased to suitable levels by doping in an amphiprotic acid [35]. There are two secondary amine sites at which acid can chemically bond to the polymer chain. PBI is typically doped such that there is both bonded acid and additional free acid present in the polymer. Bouchet *et al.* [36] showed that protons in acid-doped PBI membranes "hopped" through the membrane along chains of anionic species. The anionic species play a much greater role in conductivity than the nitrogen groups on the polymer backbone, and for this reason the conductivity of the membranes increases as the acid doping level is increased. Figure 7 shows Bouchet *et al.*'s proposed proton conduction mechanism.

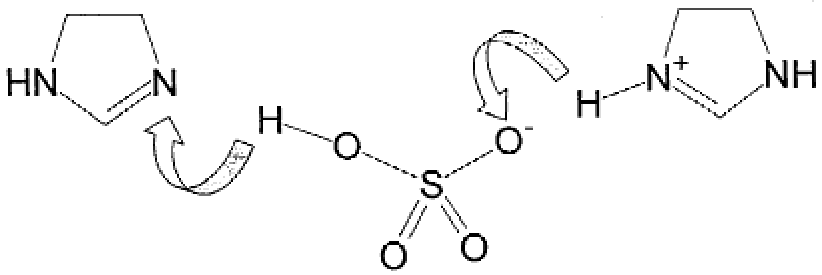

Figure 7: Bouchet *et al.*'s proposed "proton hopping" mechanism for proton conduction through acid-doped PBI membranes [36]

Along with possessing increased conductivity with respect to undoped PBI, phosphoric acid doped PBI has some other interesting characteristics. Notably, it has a water drag coefficient of close to zero [37]. The water drag coefficient indicates the number of water molecules that are pulled through the electrolyte membrane with every proton. Nafion® membranes have relatively higher water drag coefficients and extensive humidification systems are required to maintain constant operational hydration levels. Humidity does, however, also increase the conductivity of phosphoric acid-doped PBI membranes. H_3PO_4-doped PBI's conductivity at 30% relative humidity (RH) has been shown to be more than twice as high as the conductivity at 5% RH (with all other operating conditions fixed) [38]. However, phosphoric acid-doped PBI fuel cells running on completely dry gases also demonstrate excellent performance [39][40]. A series of polarization curves for commercial phosphoric acid-doped PBI MEAs are given in Figure 8. The cells are operated at ambient pressure at constant air and hydrogen stoichiometries of 2 and 1.5 with no humidification of gases.

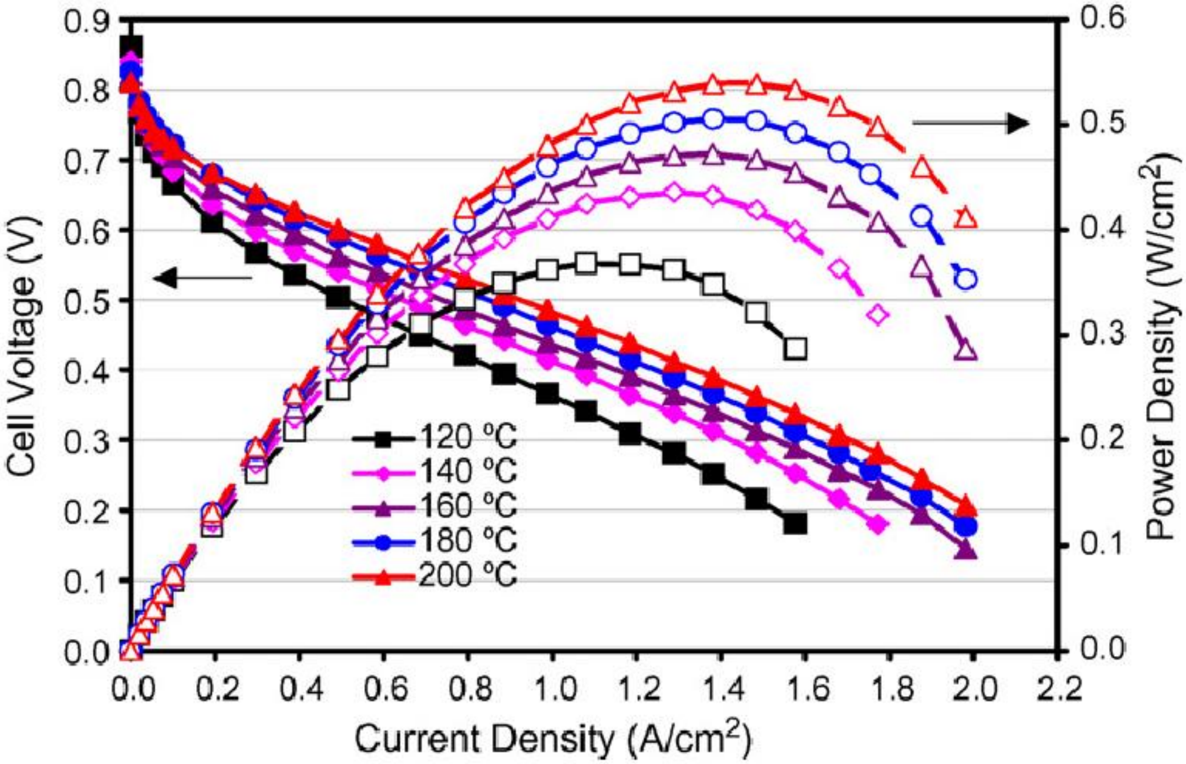

Figure 8: Performance and power density of commercial phosphoric acid-doped PBI MEAs. Dry hydrogen and air gas was fed to the fuel cells at constant stoichiometries of 1.5 and 2 respectively [41].

2.3.1 Phosphoric Acid Doping of Polybenzimidazole Membranes

PBI membranes can be made into proton conducting electrolytes by doping with phosphoric acid. Li *et al.* [42] doped PBI membranes by immersing them in phosphoric acid solutions of various concentrations. Membranes were left in solution for between 4 and 5 days at room temperature. It was found that the acid uptake into the membrane was a function of the solution concentration. Figure 9 shows the relationship between acid solution concentration and resulting doping level as found by Li *et al*.

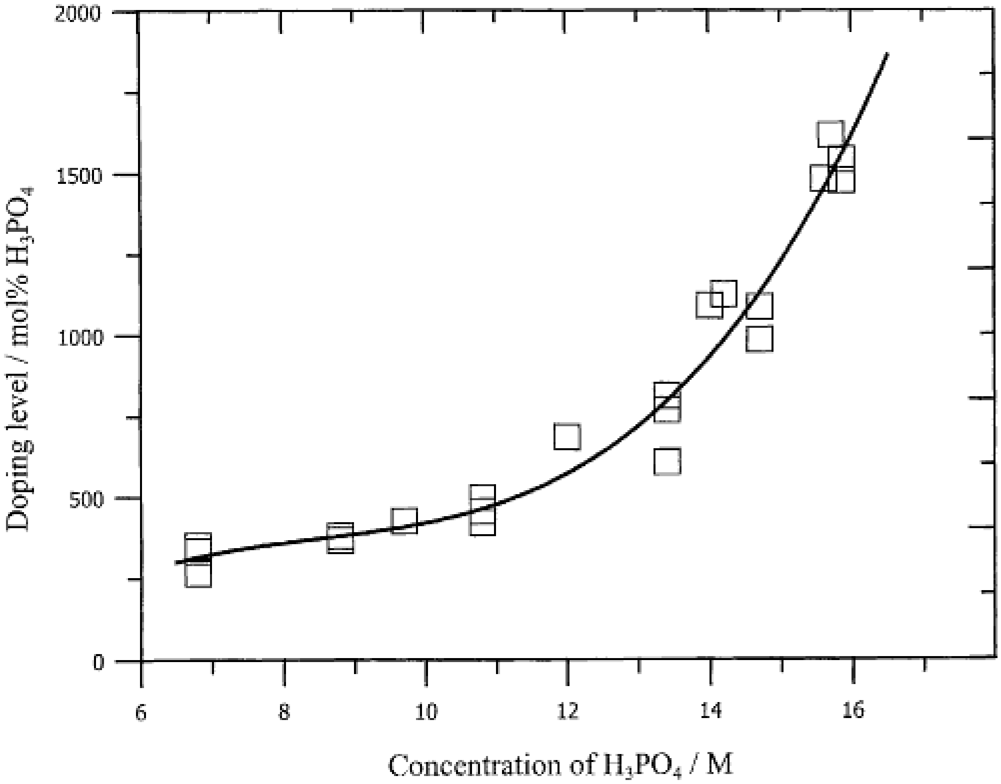

Figure 9: Phosphoric acid doping level of PBI membranes after 4- 5 day room temperature immersion in phosphoric acid solution of various concentrations [42].

Membrane durability is significantly decreased by the acid doping, especially at higher doping levels. Li *et al.* [42] tested the tensile strength of acid-doped PBI membranes of various doping levels, and proposed that a balance between membrane conductivity and durability was achieved at a doping level of 5-6 mol H_3PO_4/ repeat unit PBI.

2.3.2 Fabrication of Polybenzimidazole Membrane Electrode Assemblies

Fuel cell membrane electrode assemblies are comprised of three important regions, as shown in Figure 10.

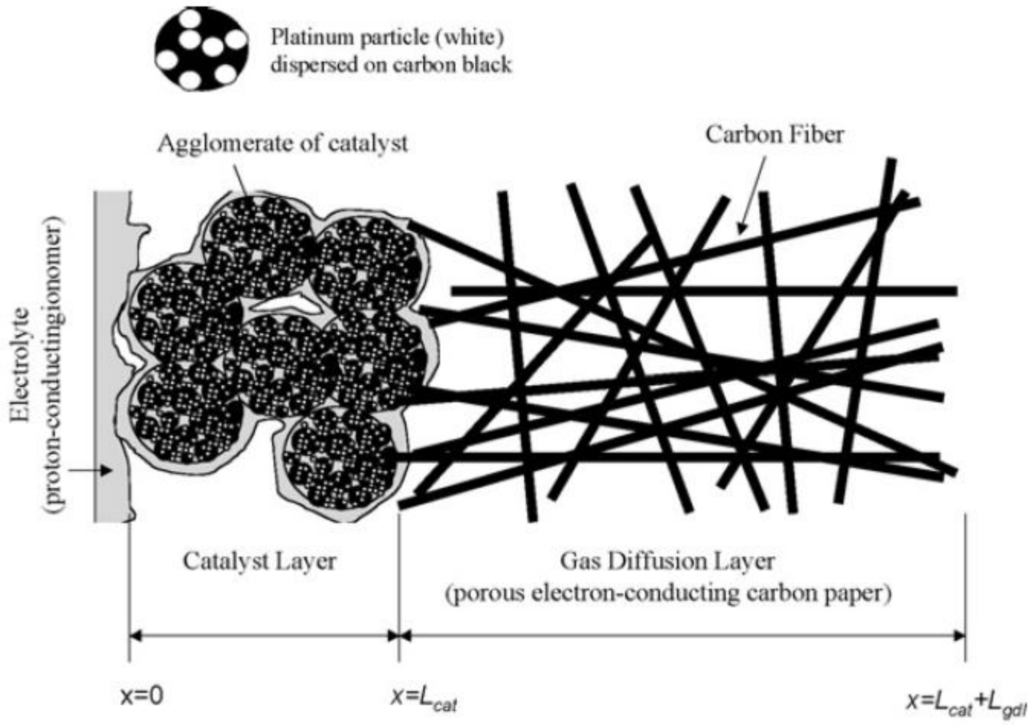

Figure 10: Regions of the 5-layer fuel cell membrane electrode assembly [43]

The three regions of the 5-layer fuel cell MEA, as shown in Figure 10, are the electrolyte membrane, the catalyst layer, and the gas diffusion layer. In a 5-layer MEA, the catalyst is applied directly to the electrically conductive gas diffusion layer to make a gas diffusion electrode. This electrode is then pressed to the membrane to make an MEA. It is assumed that good contact between the carbon gas diffusion layer and the catalyst particles is achieved, allowing uninterrupted electron flow from the current collectors. The 5-layer MEA differs from the 3-layer MEA in which catalyst is applied directly to the membrane. Fuel cell electrochemical reactions can only occur at the interface of membrane, catalyst particle and carbon layer, known as the triple phase boundary. At the triple phase boundary, protons arrive through the membrane, electrons arrive through the carbon structure, and the reaction proceeds on the catalyst site. Proper electrode fabrication plays an important role in the correct distribution of the catalyst particles and carbon layers, but MEA fabrication methods are also important. Sufficient pressure to bring the catalyst layer into intimate contact with the membrane is required, but excessive pressure can damage the MEA during fabrication.

There are many ways to prepare membrane electrode assemblies for fuel cell use. Many research groups have prepared inhouse PBI-impregnated gas diffusion electrodes and hot-pressed them to PBI membranes to form MEAs. The methods for producing the electrodes and the hot-pressing time length, applied pressure and temperature have varied significantly. Seland *et al.* [44] doped PBI-impregnated gas diffusion electrodes by spraying them with a phosphoric acid solution. These electrodes were then hot-pressed to acid-doped PBI membranes at a pressure of 2.45 MPa and a temperature of 130°C for 25 minutes. Kongstein *et al.* [45] also doped PBI-impregnated electrodes by spraying them with a phosphoric acid solution. These electrodes were then hot-pressed to acid-doped PBI membranes at a pressure of 2.5 MPa and a temperature of 130°C for 25 minutes. Li *et al.* [46] prepared PBI-impregnated gas diffusion electrodes using phosphoric acid as a solvent, which essentially doped the electrodes during manufacture. The electrodes were then hot-pressed to acid-doped PBI membranes using a pressure of 9.81 MPa and a temperature of 200°C for 10 minutes. Cho *et al.* [39] prepared PBI-impregnated gas diffusion electrodes and doped both the electrodes and the membrane in a solution of phosphoric acid. MEAs were then prepared by hot-pressing acid-doped membranes and electrodes together at a pressure of 19.6 MPa and temperature of 120°C for 3 minutes.

Oono *et al.* [47] did not hot-press electrodes to the membrane. Phosphoric acid-doped PBI membranes and undoped Pt/C electrodes with no PBI impregnation were inserted into the fuel cell hardware and compressed during cell assembly. Wainwright *et al.* [48] also used undoped Pt/C electrodes in their phosphoric-acid doped PBI membrane fuel cells. Unfortunately MEA fabrication methods were not specified for their work, however, a later article by the same group (Wang *et al.* [49]) on the use of phosphoric acid-doped PBI as a membrane for direct methanol fuel cells used a hot-pressing pressure of 22 MPa and a temperature of 150°C for 10 minutes. The Pt/Ru electrodes that were used did not contain any PBI ionomer.

2.3.3 Performance Degradation of Phosphoric Acid-Doped Polybenzimidazole Fuel Cells

It has been observed that phosphoric acid is progressively leached out of acid-doped PBI fuel cell membranes during their operation. Zhai *et al.* [50] conducted a 500 h performance degradation test on a phosphoric acid-doped PBI fuel cell. By measuring the acid content of the fuel cell effluent streams they found that acid was indeed leached from the cell during normal operation, however, the increase of the membrane resistance over the testing period was very small. Analysis of the phosphorus content of the catalyst layers before and after the lifetime test showed a substantial loss of acid content. Zhai *et al.* measured the steady performance degradation rate to be approximately 0.18 mV/h. They attributed the degradation to both the agglomeration of the catalyst particles as well as the loss of phosphoric acid from the catalyst layer of the MEA.

2.4 Electrochemical Impedance Spectroscopy Analysis of Fuel Cells

In electrochemical impedance spectroscopy (EIS) a sinusoidal voltage perturbation is applied to the system to be studied and the current response is observed [51]. This analysis is conducted over a range of perturbation frequencies, and the time-dependant resistance (called the impedance) of the system is measured at each frequency. Unlike resistance, however, impedance has both a real and an imaginary component. A plot of real impedance versus imaginary impedance is called a Nyquist plot; these plots are often used to present fuel cell EIS data. A Nyquist plot showing some typical attributes of EIS diagnostic results is given in Figure 11.

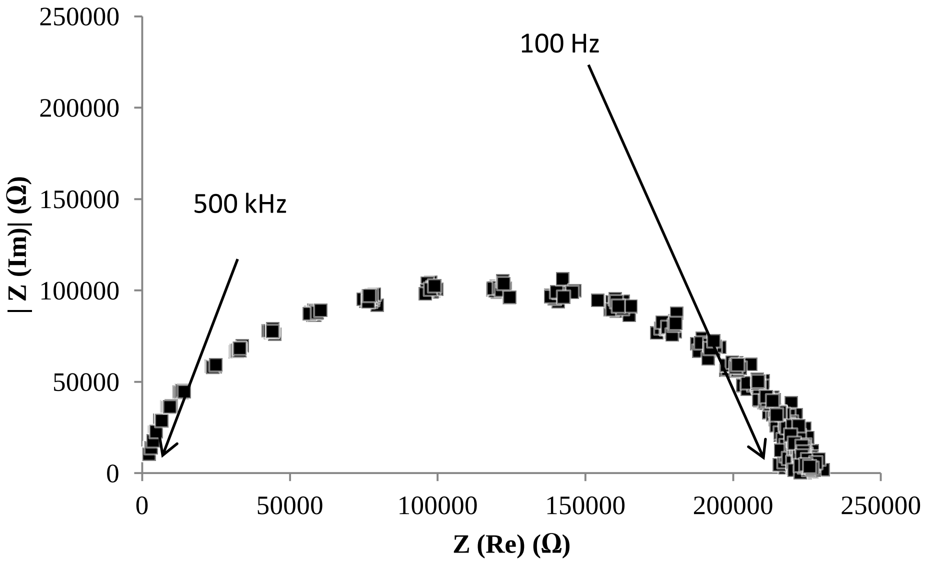

Figure 11: Nyquist plot of a PBI membrane immersed in an organic liquid [52].

The EIS data given in Figure 11 was not obtained from fuel cell analysis; it illustrates, however, a number of features that *are* typically observed in the EIS spectra of fuel cells. It was recorded for a phosphoric acid-doped PBI membrane that had been immersed in propiophenone in work by a summer intern that will be discussed later in this document. The resistance of a fuel cell's hardware (including the wires, contact resistances between the various components, etc.) is entirely ohmic, and appears only on the X-axis of the Nyquist plot. This is observed at a sufficiently high frequency during EIS, and the smallest X-intercept of the Nyquist plot gives the fuel cell membrane resistance (measured in ohms). Analysis of the semicircular impedance response of the system can provide a great deal more information on electrochemical reaction kinetics, mass transport and other phenomena.

Chapter 3 Systems Analysis and Experimental Design

3.1 Modelling of Thermally Regenerative Fuel Cell System

The TRFC hydrogenation system was modelled in a process simulation software package (UniSim®) before any experimental TRFC was completed. Propiophenone was not found within the UniSim® component database. It was decided that model compounds would be used in the place of propiophenone and 1-phenyl-1-propanol in the simulation, assuming that structural similarity would lead to thermodynamic and behavioral similarity between the model and process compounds. The compounds used to model propiophenone and 1-phenyl-1-propanol were acetophenone and 1-phenylethanol respectively, which are shown in Figure 12.

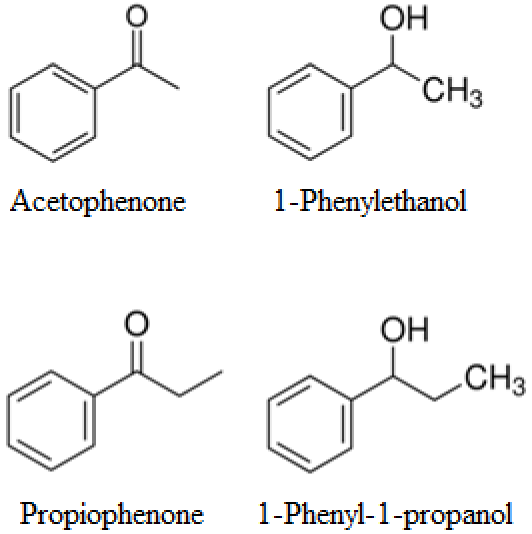

Figure 12: Model and process compounds

An equilibrium reactor was used to determine the dehydrogenation equilibrium conversion for various reactor temperatures. The model predicted that although at higher dehydrogenation temperatures the equilibrium shifted in favour of the production of acetophenone (propiophenone), the reactor effluent vapour phase fraction was very high. These results are displayed in Table 2. These results are for the model compounds, and not the process compounds, and the boiling points of propiophenone and 1-phenyl-1-propanol are close to 218°C as compared to 204°C for the model compounds. It was also assumed that there was no pressure drop or temperature loss through the system. At reaction temperatures 30°C below the boiling point of the model compounds, the vapour phase is essentially pure hydrogen, but some separation will still be required to ensure the working compounds are not progressively purged from the system.

Table 2: Reaction equilibrium conversion and vapour and liquid molar flowrates as a function of temperature

Reaction Temperature (°C)	Equilibrium Conversion (%)	Vapour Molar Flow Rate (mol/min)	Liquid Molar Flow Rate (mol/min)
140	10	0.2151	1.985
150	14.81	0.3345	1.962
160	21.41	0.5162	1.912
170	30.16	0.7963	1.807
180	41.28	1.24	1.585
190	54.59	1.983	1.109
200	69.29	3.384	0.002

As can be seen in

Table 2 a maximum equilibrium conversion of approximately 70% was predicted at 200°C. At that temperature the reactor effluent was essentially all vapour, and separating the hydrogen from the alcohol and ketone vapour components would become very difficult. A much lower equilibrium conversion was predicted at lower reaction temperatures, but a smaller fraction of the model compounds entered the vapor phase, and separation would be easier. Only the scenario resulting in the highest equilibrium conversion was studied in depth, and the system was modelled using a dehydrogenation reactor temperature of 200°C. The reactor effluent required a condenser to remove the vaporized working compounds from the hydrogen stream.

Figure 13 shows the vapour phase mole fractions of the condensed reactor effluent at various condenser temperatures.

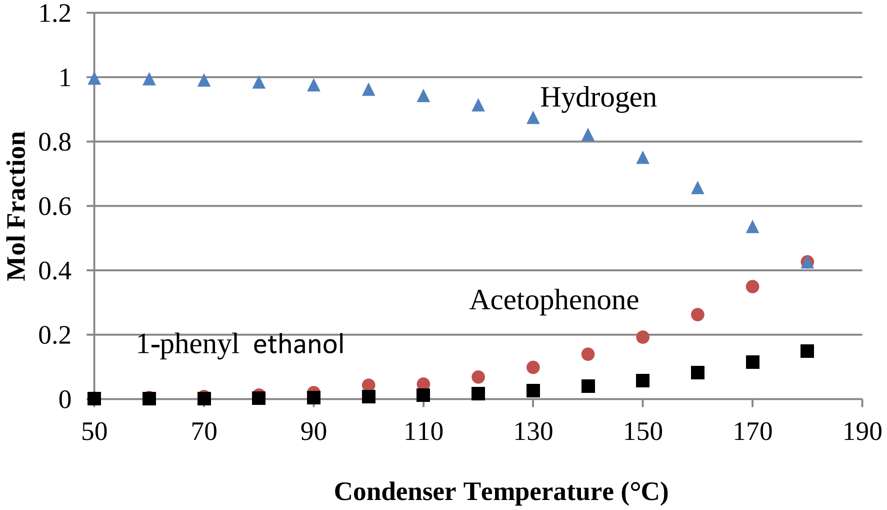

Figure 13: Reactor effluent vapour phase mol fractions as a function of condenser temperature

Figure 13 shows that operating the dehydrogenation reactor at the maximum equilibrium conversion is likely not the ideal solution. Condensing the working substances from the reactor effluent would require a condenser operating at a low temperature relative to both the fuel cell and the dehydrogenation reactor. This could complicate the TRFC system, but it is potentially still possible if efficient use can be made of the waste heat from the energy source.

In the current design of the TRFC there is no exit from the anode. Propiophenone and 1-phenyl-1-propanol that arrive at the anode would remain there, flooding the electrode. Separation of the dehydrogenation products would allow for a simple recycle of the working substances back into the dehydrogenation reactor, but this was beyond the scope of this project and must be considered in future work.

3.2 Thermally Regenerative Fuel Cell Thermodynamic Cell Potential

The thermodynamic open circuit voltage of the TRFC system was estimated from the Gibb's free energy change of the hydrogenation reaction using van't Hoff plots generated from equilibrium data collected during concurrent work by another student at Queen's working on the TRFC project [18]. The van't Hoff plot and calculated ΔH° and ΔS° values for the hydrogenation reaction of propiophenone are shown in Figure 14 and the calculated Gibb's free energy change of the hydrogenation reaction and ideal cell voltages at various temperatures are reported in Table 3. Sample calculations are presented in the Appendix. The calculated ideal cell voltages assume that ΔH° and ΔS° are invariant with temperature.

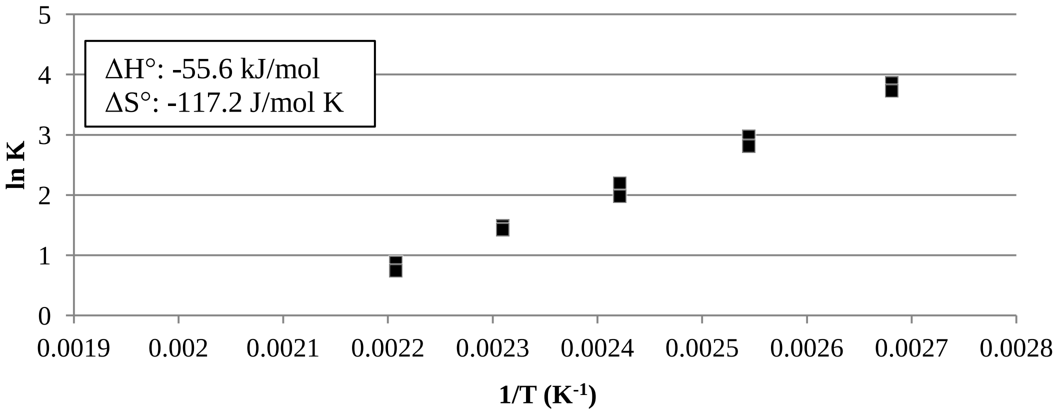

Figure 14: Van't Hoff plot for the dehydrogenation of 1-phenyl-1-propanol (data from [18])

Table 3: Calculated ideal cell potentials for the hydrogenation of propiophenone at various temperatures

Temperature (K)	ΔG_{rxn} (kJ/mol)	E_{cell} (mV)
373	-11.9	61.6
393	-9.5	49.5
413	-7.2	37.3
433	-4.9	25.1
453	-2.5	13
473	-0.2	0.9

The equilibrium data used to generate the thermodynamic cell voltages presented in Table 3 were obtained during the catalyzed chemical dehydrogenation of 1-phenyl-1-propanol, and are not necessarily representative of the electrochemical TRFC system's cell potential. However, as calculated the TRFC system will have a very low open circuit potential at the intended operating temperatures between 140°C and 160°C.

3.3 Apparatus

3.3.1 Fuel Cell Assembly Hardware

Fuel cells were assembled using anodized aluminum fuel cell end plates and gold-coated copper current collectors. Current collectors were electrically insulated from the end plates using fibre-reinforced Teflon gaskets.

Flowfield plates made from a graphite/aromatic thermoplastic polyester composite material were used to channel fuel and oxidant flow across the surfaces of the electrodes. The flowfield plates were manufactured with double serpentine channels and had channel dimensions of 1mm x 1mm. For most MEAs the flowfield plates that were used had channels that covered an area of 6.25 cm^2, but flowfield plates with 25 cm^2 channel areas were used to test MEAs with larger electrodes.

Fuel and oxidant flows were directed from the fuel cell end plates to the flow field plates through Teflon tubes.

Reinforced silicone gaskets were initially used to seal the fuel cell. This material, however, was not compatible with the acid-doped polybenzimidazole membranes that were used. Teflon was found to be suitable for the temperatures and materials in the cell and later tests used this material for sealing. Gaskets were cut to fit the flow field plates. The thickness of the gasket was approximately 80% of that of the carbon backing paper which gave good electrical contact between the flowfield plates and the electrodes.

3.3.2 Hydrogen-Air Baseline Membrane Electrode Assembly Testing

A Hydrogenics fuel cell testing station (Model# G60) was used to measure the baseline hydrogen-air polarization curves for PBI MEAs that were fabricated inhouse. Although the performance of the PBI MEAs with dry gases would have provided a more useful comparison to the performance in the anhydrous environment of the TRFC, the flow path of the gases in the G60 test station passes through a humidification chamber that required a minimum water level for the system to operate. Typically the minimum water temperature in the humidifier was 25°C, which lead to a relative humidity of approximately 3% at the test temperature of 160°C. The Hydrogenics test station controlled and recorded data for gas flow, gas temperature, gas humidification, fuel cell temperature and current. The cell voltage was measured and recorded at various current densities to generate polarization curves.

3.3.3 Propiophenone Hydrogenation Cell Test System

The development of a suitable test system for the TRFC was a primary objective of this project. The design, assembly and commissioning of this test station represented a significant portion of the work of this graduate project. An image and a schematic of this test system are presented in Figure 15 and Figure 16 respectively.

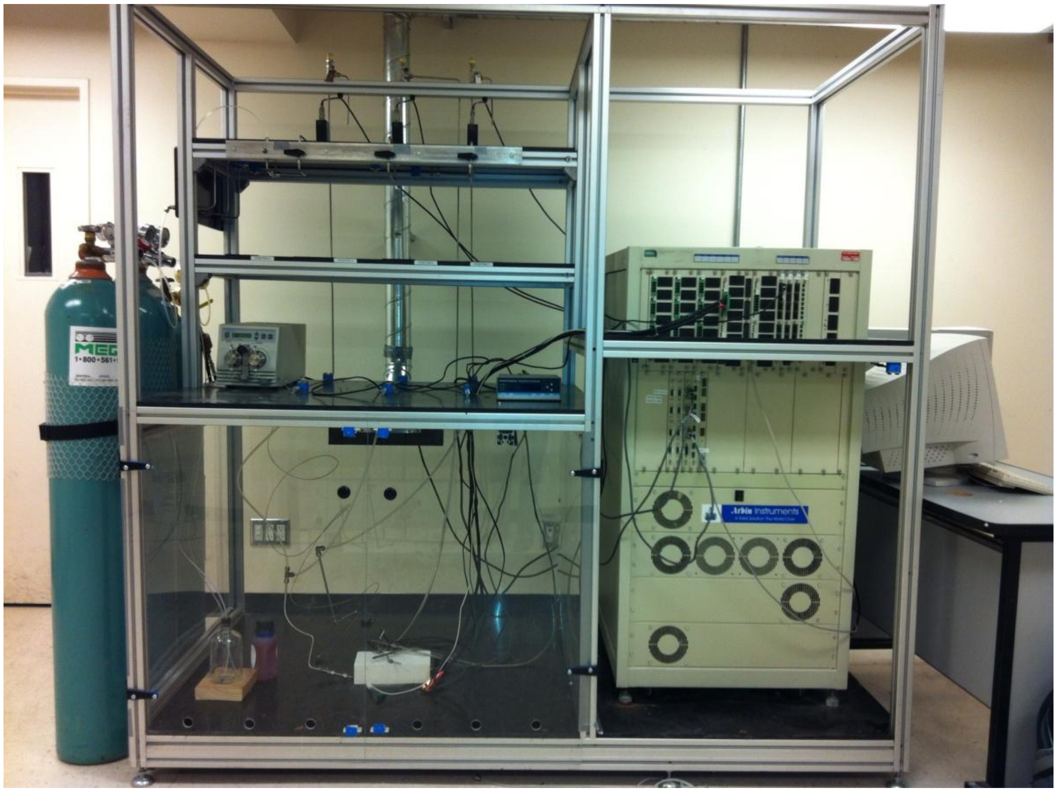

Figure 15: Thermally regenerative fuel cell testing system

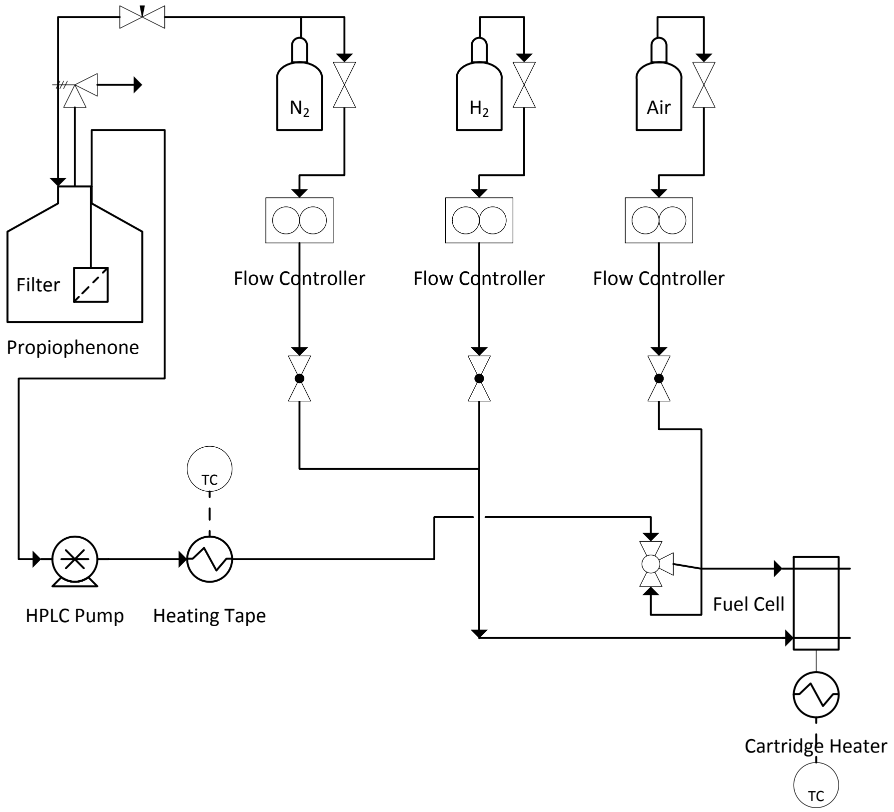

Figure 16: Schematic diagram of thermally regenerative fuel cell test system

Many materials used in the construction of the TRFC system were repurposed from an existing direct methanol fuel cell system, with very few new materials being required. The aluminum scaffolding that had supported the direct methanol fuel cell test station was reused for the TRFC system after removal of unnecessary components was completed. Two mass flow controllers from the existing system were reused in the TRFC along with many Swagelok fittings and lengths of stainless steel tubing. An Arbin BT-2000 multi-channel battery testing station provided load and gas flow control as well as data acquisition capability for the TRFC test station.

The flow rate of the DMFC system's pump was controlled by manually setting the stroke rate and length. This pump did not provide steady flow and it was very difficult to set and measure its flow rate, especially at low flow settings, and it was therefore removed from the scaffolding. A high pressure liquid chromatography pump was obtained and calibrated at low flow rates (as low as 0.01 mL/min) using a stopwatch and a graduated cylinder.

It was assumed that gas flow would be rapidly brought to temperature inside the fuel cell without needing preheating. The stainless steel tubing through which propiophenone was fed to the fuel cell was wrapped in a ribbon heater for several feet and thoroughly insulated. The fuel cell itself was heated using two cartridge heaters. Temperatures for the fuel cell and the propiophenone feed line were individually controlled using temperature controllers and thermocouples.

Hydrogen, air and nitrogen gas cylinders were obtained and secured to the scaffolding. Stainless steel tubing and Swagelok fittings routed gas from the cylinders to the mass flow controllers. Valves were installed preceding the mass flow controllers for an easily accessible gas shut-off point. Stainless steel tubing was installed following the mass flow controllers to bring the gases to the fuel cell.

A septum-sealed glass jar was used as a reservoir for propiophenone. To keep the reservoir as air-free as possible, a needle valve was used to control a constant bubble of nitrogen through the reservoir. A needle inserted through the reservoir’s septum seal provided pressure release. An in-line filter was attached to the liquid line inside the propiophenone reservoir to protect the HPLC pump.

The system was designed to provide either hydrogen (fuel) or nitrogen (to enable purging) to the anode of the fuel cell. The cathode of the fuel cell could be provided either air (for testing as a conventional fuel cell) or propiophenone (for testing as a TRFC), depending on the inlet that was attached.

Propiophenone was collected at the cathode outlet of the fuel cell for future chemical analysis. Hydrogen and air were directed to the ventilation outlet inside the test system.

Propiophenone and 1-phenyl-1-propanol are combustible and their vapours are irritating to mucous membranes and skin [53][54]. To limit researcher exposure to fumes a Plexiglas enclosure was built into the scaffolding and connected to the laboratory's fume cupboard ventilation system. For the HPLC pump to draw sufficient head the propiophenone reservoir had to be kept physically more elevated than the pump and was therefore kept outside of the ventilated enclosure. All gas lines were red into the ventilated enclosure and fuel cells were tested there as well. All gas and vapour removed by the ventilation was passed through the Queen's University gas scrubbing system.

3.3.4 Propiophenone Feed and Heating Control System

A Waters high-pressure liquid chromatography pump (Model# 515) was used to deliver propiophenone to the anode of the fuel cell. The Model# 515 has a flow rate range of 0.000-10.000 mL/min in 0.001 mL/min increments. The flow rate accuracy is ±1.0 % of setting (measured using degassed methanol at a flow rate of 1 mL/min and operating between 1000-2000 psi backpressure) and the flow rate precision is ±0.1% (measured at a flow rate of 1 mL/min and operating between 1000-2000 psi backpressure). The effect of pressure change on flow rate is ≤2.0% when using degassed methanol at a flow rate of 1 mL/min and operating at 1000 psi backpressure. 99% purity propiophenone was used in all experiments. Propiophenone flow was delivered to the fuel cell through a 90 cm length of 1/8" stainless steel tubing wrapped with heating tape.

3.3.5 Temperature Control

The fuel cell end plates and the propiophenone feed line were both heated to allow testing at temperatures between 40°C and 200°C. The propiophenone feed line was heated with heat tape connected to a Barnant Company temperature controller (Model# 689). The feed line temperature was monitored using a J-type thermocouple wrapped beneath the heating tape.

The fuel cell end plates were heated using two cartridge heaters; one heater was inserted into each of the anode and cathode end plates. The heaters were controlled by a Barnant Company temperature controller (Model# 689). The fuel cell temperature was monitored using a J-type thermocouple inserted into the cathode end plate. The temperature difference between the two end plates was measured and found to be negligible. The Model# 689 has an accuracy of ±0.4°C when using a Type-J thermocouple at temperatures above 173K.

3.3.6 Gas Feed and Flow Measurement

Hydrogen (UHP grade), air (UHP) and nitrogen (oxygen free) feed gases were supplied from gas cylinders at flow rates controlled by MKS Instruments Mass Flo® mass flow controllers (Model# 1179A). The 1179A has an accuracy of ±1% of the flow setting including non-linearity and non-repeatability referenced to 760 mmHg and 0°C. Mass flow controller set points could be specified via the Arbin battery test system software and the mass flow was also monitored and recorded by the Arbin data acquisition system.

3.3.7 Analysis of Hydrogenation Products

A Shimadzu gas chromatograph (Model# GC-17A) was used to analyze the hydrogenation products of the TRFC cathode. An Agilent column with DB-5 packing material and dimensions of 30m x 0.25 mm x 0.25 microns, and temperature limits between -60°C and 350°C. The temperature program that was used is given in Table 4.

Table 4: Temperature profile used for gas chromatograph analysis

Step Number	Start Temperature (°C)	Final Temperature (°C)	Ramp Rate (°C/min)	Hold Time at Final Temperature (min)
1	70	90	15	1
2	90	120	10	2
3	120	230	10	1
4	230	70	40	0

3.4 Membrane Electrode Assembly Preparation

3.4.1 Electrodes

Two different types of electrodes were used in the preparation of the MEAs used in this experimental work. Pt/carbon paper electrodes (Electrochem) with 20 wt% catalyst loading (1mg Pt/cm^2) were used in the fabrication of initial membrane electrode assemblies (MEAs). Carbon cloth ionomer-coated PBI electrodes with a platinum loading of 1 mg/cm^2 (Danish Power Systems) were also obtained and used in the fabrication of MEAs.

3.4.2 Polybenzimidazole Membranes

The PBI membranes used in this experimental work were manufactured by Danish Power Systems of Copenhagen, Denmark. Sheets of meta-PBI synthesized from N,N-diaminobenzidine and isophthalic acid in polyphosphoric acid with a molecular weight and thickness of approximately 45,000 g/mol and 40 µm respectively were obtained and used in MEA fabrication.

3.4.3 Acid Doping of Polybenzimidazole Membranes

The method used to dope polybenzimidazole membranes with phosphoric acid is based on Li *et al.* [42]. Membranes were weighed then immersed in phosphoric acid of various concentrations. After 72h of immersion the acid-impregnated membranes were removed from solution, blotted dry and placed into a vacuum oven at 100°C for 24h. Membranes were dried in the oven until successive weighings showed no further weight loss. It was assumed that all water was removed during the drying process and that measured weight gain was due entirely to phosphoric acid uptake. Membrane doping level (DL) was calculated as the number of mols of phosphoric acid taken up by the membrane divided by the number of mols of repeat units of polybenzimidazole in the membrane sample.

3.4.4 Polybenzimidazole Impregnation of Electrodes

Electrodes were impregnated with polymer electrolyte to increase their performance. A 2 wt% solution of PBI in dimethylacetamide (DMAc) was prepared from PBI powder with an approximate MW of 67,000 g/mol (based on the specifications provided by the manufacturer, Danish Power Systems). The polymer was dissolved into DMAc and sprayed onto pre-cut platinum on carbon electrodes in even coats using an air-powered spray gun. Coated electrodes were placed into a vacuum oven at 100°C for 20h to volatilize and remove DMAc. Electrodes were left in the oven until successive weighings showed no further weight loss. The spraying procedure was repeated until the polymer loading approximately matched the values used by the Bjerrum group at Danish Technical University (0.7 mg/cm^2) [55].

3.4.5 Acid Doping of Polybenzimidazole-Impregnated Electrodes

PBI-coated electrodes were doped with phosphoric acid using an air-powered spray gun. 1M phosphoric acid was used to completely cover the surface of the electrodes. Water was removed from the electrodes in a vacuum oven at 105°C until consecutive weighings showed no further change (approximately 20 hours). The spraying procedure was repeated until the acid loading approximately matched Lobato *et al.'s* value of 0.5 mg/cm^2 [56].

3.4.6 Hot Pressing of Membrane Electrode Assemblies

Membrane electrode assemblies were hot-pressed using a Carver Hydraulic Unit (Model# 3925). The Carver press was fitted with two heated platen, each individually heated by cartridge heaters. Platen temperature was controlled by Barnant Company temperature controllers (Model# 689). Membranes and electrodes were sandwiched between electrodes and placed between two other plates (referred to hereafter as hot-pressing plates). The materials of the hot-pressing plates were varied during experimental work. Hot-pressing plates containing membranes and electrodes were then placed between the platen and compressed. Hot-press duration, temperature and force were selected based on literature values [39][45][46].

3.4.7 Commercial Membrane Electrode Assemblies

Commercial phosphoric acid-doped polybenzimidazole MEAs (Dapozol®, Danish Power Systems) were obtained and used in this experimental work. The acid doping level of the membranes and the ionomer and acid content of the electrodes was not provided by the manufacturer. The catalyst loading of the anode and cathode respectively was 0.33 mg/cm^2 and 1.07 mg/cm^2.

3.5 Fuel Cell Assembly and Performance Testing

3.5.1 Fuel Cell Assembly

The MEA to be tested was placed between two flow-field plates with machined double serpentine flow-fields. The perimeter of the MEA was sandwiched between flat gaskets that formed an approximately 1 cm wide seal between the flow-field plate and the PBI membrane. End plates were attached to each other using 8 bolts and the cell was placed under a load of approximately 2000 lb using an Enerpac hydraulic press (Model# RC1010). After compressing the cell the bolts were tightened to 55 inch-pounds using a torque wrench.

Immediately following cell assembly the through-plane resistance between the two current collectors was measured using a Hioki milliohmmeter (Model# 3560AC). Cell resistance was used to check for proper assembly and cells with resistances over 2Ω were typically disassembled, checked for alignment and then reassembled. Fuel cells were also checked for crossover leaks using nitrogen gas at a differential pressure of 1barg and those found to have leaks were disassembled, checked for correct gasket alignment and membrane damage, and subsequently reassembled if the problem could be rectified.

3.5.2 Hydrogen-Air Fuel Cell Performance Testing

Hydrogen-air fuel cells were tested using both galvanostatic and potentiostatic methods. Voltage and current control and data acquisition was accomplished either using an Arbin multi-channel battery testing station (Model# BT2000) or a Hydrogenics fuel cell testing station (Model# G60).

Gas flow was initiated and fuel cells were heated to the desired temperature before any current was drawn. Fuel cells were tested at temperatures between 100°C and 160°C, typically starting with low temperature tests before heating the cells further. Each test point was held until constant performance was observed for two minutes. Gas flow rates were kept constant in most cases. Each fuel cell was tested multiple times at each set of conditions to determine the reproducibility of the results.

3.5.3 Thermally Regenerative Fuel Cell Performance Testing

A set of passive resistors was used to impose a set resistance across the thermally regenerative fuel cell. Voltage was monitored using the Arbin testing station, and it was assumed that all resistance in the circuit was due to the passive resistor. Ohm’s law was used to calculate the current that was flowing through the circuit. Each resistance was maintained across the circuit until a stable voltage was observed for two minutes. Polarization data was obtained first at low current densities using large resistors followed by progressively lower resistances until a limiting current was reached. Resistors were changed manually.

Hydrogen and propiophenone flow were initiated and the system was heated to the set point before any current was drawn.

3.5.4 Conductivity Testing of Phosphoric Acid-Doped Polybenzimidazole in Propiophenone

Ex-situ electrochemical impedance spectroscopy was used to measure the in-plane conductivity of phosphoric acid doped PBI immersed in propiophenone. The procedure was based on a previously developed method from the literature by Holdcroft *et al.* [57] in which the conductivity of Nafion® membranes immersed in water were analyzed. A Nylon support was built to hold the membrane in place during testing and contact the membrane edges to two platinum electrodes held 2.4 cm apart. EIS was conducted using voltage perturbations of ± 5 mV across a voltage of 0V. A frequency range of 500 kHz to 100Hz was used and test temperatures ranged from 80°C to 140°C.

The membranes used in these trials were PBI membranes that have been used elsewhere in this experimental work (Danish Power Systems) and were doped in phosphoric acid before being tested.

The Nylon support was immersed in a propiophenone bath that itself was immersed in an oil bath. The propiophenone bath was partially covered to limit evaporation and was suspended above the base of the oil bath to allow better oil circulation. The oil bath was stirred using an electric impeller and heated on a hot plate.

Chapter 4 Results and Discussion

4.1 Selection of Membrane

An extensive review of the literature pertaining to non-aqueous membranes was conducted in order to find materials that were suitable for the proposed thermally regenerative fuel cell system and compatible with the ketone-alcohol pair. Concurrent TRFC research showed that the catalyzed chemical hydrogenation of propiophenone did not occur at sufficient rates below 100°C [18]. To reduce system complexity by operating with liquid propiophenone and 1-phenyl-1-propanol flow the maximum operating temperature of the hydrogenation reaction was determined by the boiling points of the compounds (218°C and 219°C respectively). A high temperature polymer electrolyte membrane fuel cell was selected based on the minimum and maximum hydrogenation temperatures of 100°C and 200°C respectively.

Phosphoric acid-doped PBI was chosen as a potential electrolyte membrane for the TRFC based on its unique characteristics. Thermal stability at high temperature and good chemical resistance have both been reported in the literature for undoped PBI [58].

PBI’s reported conductivity in the absence of humidification was of primary interest in this work. It was assumed that a hydrated membrane would be quickly dehydrated by the working fluids constantly flooding the cathode, and any membrane requiring water for conductivity would then be unsuitable for TRFC use.

4.2 Phosphoric Acid Doping of Polybenzimidazole Membranes

Undoped PBI is a protonic insulator. In the current experimental work, undoped PBI membranes were doped with phosphoric acid to increase their proton conductivity. The resulting acid uptake for the membranes is shown in Figure 17.

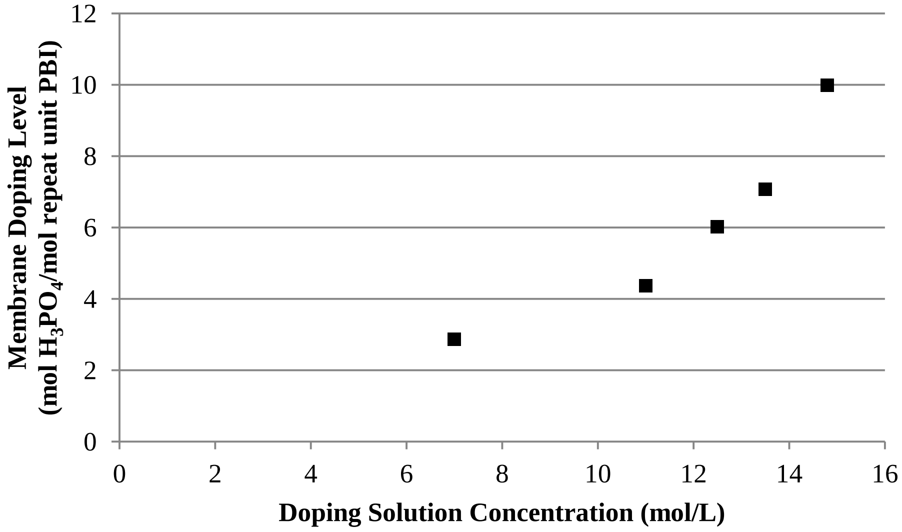

Figure 17: Average phosphoric acid uptake of PBI membranes

The resulting membrane doping levels agree well with those reported in the literature [42] [59]. Initially creation of membranes with doping levels of approximately 5-6 mol H_3PO_4 /mol of repeat unit PBI was attempted, but to achieve better performance later membranes were doped to higher levels.

4.3 H_2-Air Performance of Initial Membrane Electrode Assemblies

The method used for fabricating the initial MEAs was based on the hot-pressing method used by Kongstein *et al.* [45]. They hot pressed the electrodes onto the MEA for 25 minutes at 130°C and 2.5 MPa. It should be noted that two errors were made during the initial MEA fabrication in this experimental work. Firstly, the total force used during hot-pressing far exceeded the intended force. This was due to an incorrect assumption regarding the area over which force was distributed. Secondly, the gaskets that were used to seal the membrane to the flowfield plates could not withstand the operating conditions of the fuel cell. The consequences of these errors were rapid degradation and poor MEA performance. Different approaches were taken to solve the problems, but the true causes were not discovered until after a considerable number of MEAs had been fabricated and tested. Of the 28 MEAs fabricated during this experimental work, 4 were destroyed during hot-pressing, 2 were not performance tested because their crossover leaks could not be fixed and 18 could not be tested at temperatures in excess of 110°C without rapid performance degradation occurring.

The MEAs being produced were first evaluated by testing in hydrogen-air fuel cell conditions before TRFC conditions. A minimum acceptable performance was required: a minimum voltage of 600 mV at a current density of at least 100 mA/cm^2 was required before a cell would be tested under TRFC further. These values do not indicate high performance, but would show that the fuel cells were functioning suitably for subsequent TRFC testing.

For the initial MEA fabrication procedure, phosphoric acid-doped PBI membranes and commercial Pt/carbon paper (Electrochem) electrodes were hot-pressed together without further treatment. These initial MEAs showed poor performance in hydrogen-air and the voltage at 100 mA/cm^2 was well below 600 mV. Figure 18 is a polarization plot showing the performance of two MEAs made using membranes with doping levels of 9.8 and 3.94 mol H_3PO_4/mol repeat unit PBI. Gas flows and backpressures were set to 250 mL/min and 35 kPag respectively, and fuel cells were assembled using reinforced silicone gaskets. Both MEA#1 and MEA#2 were tested immediately following assembly and heating of the fuel cells. Maximum performance as well as hot-pressing conditions and membrane doping levels are given in Table 5.

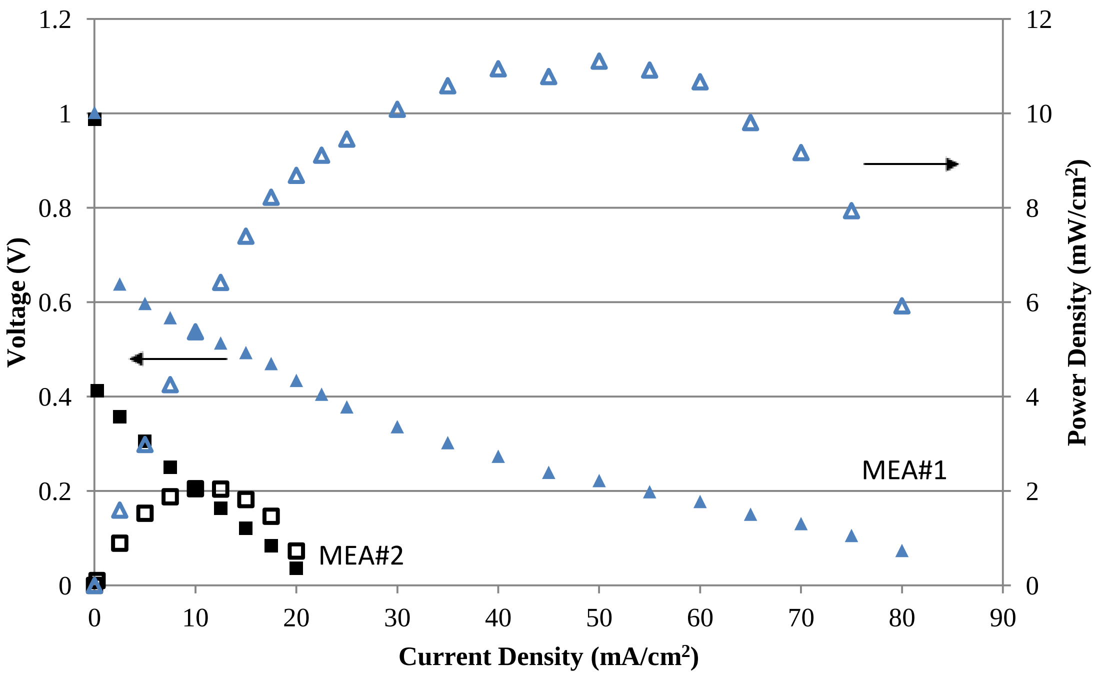

Figure 18: Performance of MEA#1 and MEA#2 at 100°C. Hydrogen and air flowrates were kept constant at 250 mL/min. Fuel cells were operated at atmospheric pressure.

Table 5: Hot pressing conditions, membrane doping levels and maximum performance for MEA#1 and MEA#2

	Doping Level (mol H_3PO_4/mol PBI)	Hot Press Time (min)	Hot Press Pressure (MPa)	Hot Press Temperature (°C)	Maximum Power Density (mW/cm^2)	Current Density at Maximum Power Density (mA/cm^2)
MEA#1	9.8	25	53.4	130	11.1	50
MEA#2	3.94	25	53.4	130	2	10

4.4 Hot-Press Plate Materials Selection

It had been noted that the electrodes of some MEAs were strongly adhering to the hot-pressing plates following hot-pressing. The adhesion was so strong that the electrodes remained firmly attached to the hot-pressing plates and detached partially from the membrane. Figure 19 shows the consequence of the adhesion of a MEA's electrode to the hot-pressing plates.

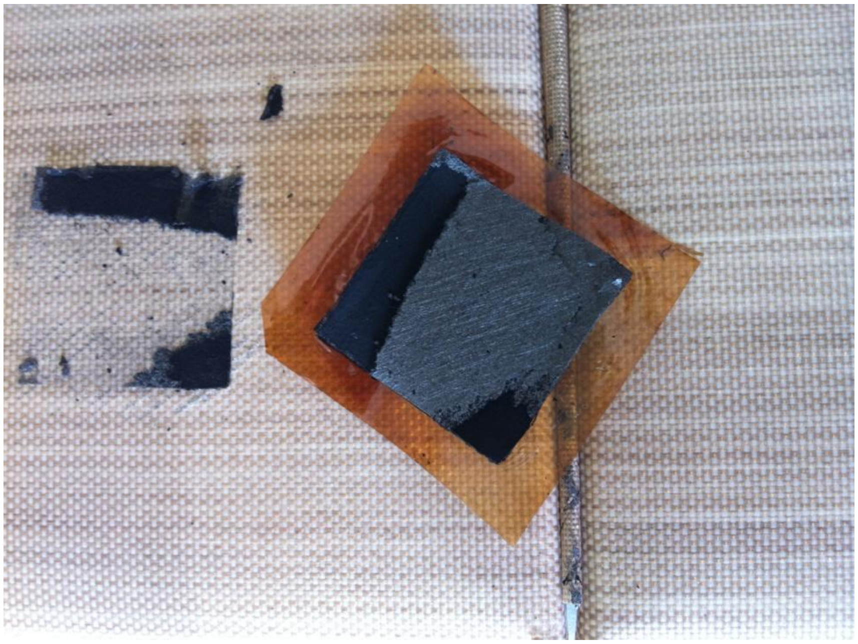

Figure 19: MEA adhesion to original silicone-covered aluminum hot-pressing plates

It was initially thought that the adhesion was related to the deterioration of the hot-pressing plates. Initial MEA fabrication used aluminum hot-pressing plates wrapped in reinforced silicone fabric. As the hot-pressing plates were used it could be seen that the smooth plastic finish of the fabric was beginning to deteriorate where contact with the MEAs had occurred. After multiple subsequent MEAs adhered and tore upon removal from the hot- pressing plates it was decided that new plate materials were required.

For each potential new material a pipette was used to place approximately 0.1 mL of 5M phosphoric acid between two 4 cm^2 pieces of carbon paper. The carbon paper was placed between the proposed hot pressing plate materials and placed in the hot-press for 25 minutes at 140°C under a pressure of 66.9 MPa. This study was designed to locate a plate material that would not adhere to the electrodes after hot-pressing at conditions similar to those used in previous trials. Gold plated copper plates were found to be the most effective for pressing the acid-impregnated carbon paper without adhesion or damage. These plates were used in the subsequent production of MEAs and significantly reduced damage to the electrodes, although the occasional MEA still adhered and was damaged. It should be noted that once the correct area of pressure distribution was accounted for and the applied force was reduced so that the pressure was consistent with that reported in the literature for hot-pressing no further MEA damage was observed and no electrode adhesion to the plates occurred.

4.5 H_2-Air Performance of Acid Doped Polybenzimidazole Membranes Using Ionomer-Coated Electrodes

It was proposed that the poor performance of the MEAs that were fabricated in-house was due to lack of proton conductivity in the electrode layer. A number of researchers in the literature have described methods for impregnating the electrocatalyst layer with ionomer in order to increase proton transport to the active catalyst sites. Ionomer-coated Pt/carbon cloth electrodes were provided by Danish Power Systems and had a catalyst loading of 1mg/cm^2. The ionomer loading was not specified. These electrodes were hot-pressed with H_3PO_4-doped PBI membranes to produce MEAs using conditions similar to those used in the hot-pressing of MEA #1 and MEA#2. Reinforced silicone gaskets were used to seal both the anode and cathode of the fuel cell. Table 6 details the membrane doping level and hot-pressing conditions used to prepare MEA#3, as well as the performance that was achieved. Figure 20 shows the H_2-air polarization curve of MEA #3 which was obtained using a Hydrogenics G60 fuel cell test station. Hydrogen and air flows were both controlled at 200 mL/min. The cell was operated at atmospheric pressure.

The performance of MEA#3 was much higher than that of the previous MEAs that had not been impregnated with ionomer.

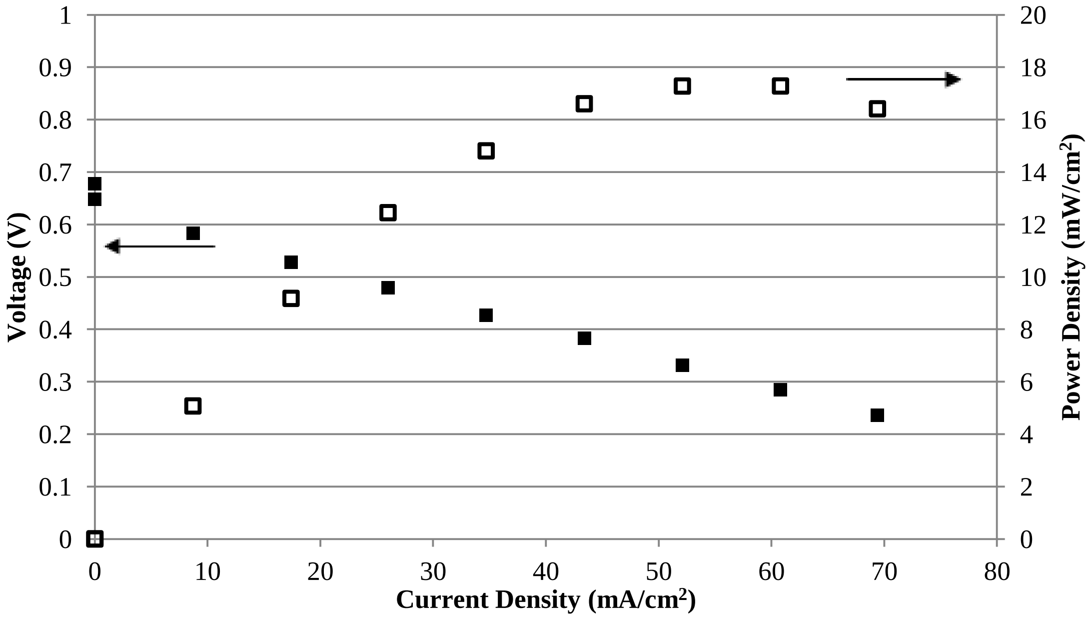

Figure 20: Performance of MEA#3 at 100°C. Hydrogen and air flowrates were held constant at 200 mL/min. The fuel cell was operated at atmospheric pressure.

Table 6: Maximum performance, hot-pressing conditions and membrane doping levels for MEA #3

	Doping Level (mol H_3PO_4/mol PBI)	Hot Press Time (min)	Hot Press Pressure (MPa)	Hot Press Temperature (°C)	Maximum Power Density (mW/cm^2)	Current Density at Maximum Power Density (mA/cm^2)
MEA#3	6.21	25	40.4	130	17.3	60.8

4.6 The Effect of Hot-Press Pressure and Temperature

In a separate effort to increase fuel cell performance Kongstein *et al.*'s [45] hot pressing conditions were modified by increasing the hot-press temperature and pressure to create a better contact between the membrane and electrodes. The error regarding the hot-pressing pressure had not yet been noted, and the applied pressures are far in excess of the literature values. Figure 21 shows the performance of four MEAs that were hot-pressed at various conditions and tested at 110°C with H_2-air. Gas flowrates were set to 200 mL/min and fuel cells were operated at atmospheric pressure on a Hydrogenics G60 fuel cell test station. Fuel cells were assembled using reinforced silicone gaskets. At the maximum current density the stoichiometric ratios of air and hydrogen were 9.8 and 2.1 respectively. Typical fuel cell air and hydrogen stoichiometric ratios are approximately 3 and 2 respectively, and flowrates were chosen to maintain the ratios in excess of these values at the maximum current density. Commercial Pt/carbon paper electrodes (Electrochem) with a platinum loading of 1mg/cm^2 were used in the making of each MEA. Table 7 gives hot-pressing conditions and doping levels for each MEA.

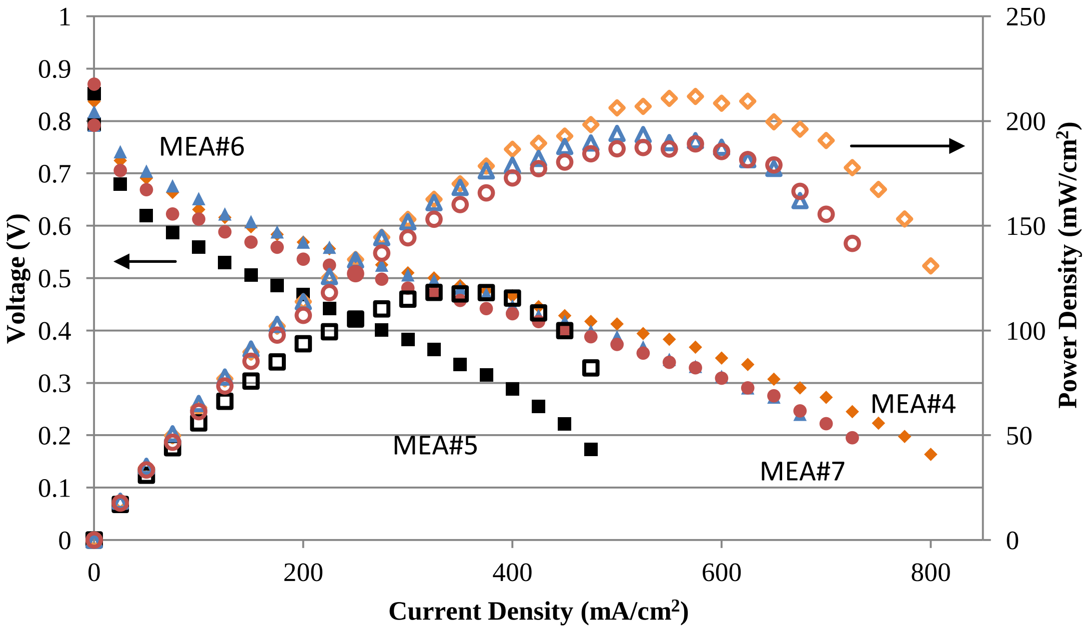

Figure 21: Performance of MEA #4, MEA#5, MEA#6 and MEA#7 at 110°C. Hydrogen and air flow rates were held constant at 200 mL/min. The fuel cell was operated at atmospheric pressure.

Table 7: Maximum Performance, doping levels and hot-press conditions of MEA#4, MEA#5, MEA#6 and MEA#7

	Doping Level (mol H_3PO_4/mol PBI)	Hot Press Time (min)	Hot Press Pressure (MPa)	Hot-press Temperature (°C)	Maximum Power Density (mW/cm^2)	Current Density at Maximum Power Density (mA/cm^2)
MEA#4	10.2	25	68.1	140	212	575
MEA#5	10.3	25	54.5	140	118	375
MEA#6	9.3	25	90.9	140	187	575
MEA#7	9.98	25	54.5	150	189	575

The performance of MEAs #4-7 was a significant improvement over previous electrode assemblies and MEA#4 achieved a maximum power density of approximately 212 mW/cm^2. This was the best performance achieved for the inhouse fabricated MEAs.

Because MEA#4 met the minimum performance threshold that has been previously described, attempts were made to produce MEAs using the same hot-pressing conditions. Each of these attempts, however, resulted in damaged MEAs that could not be tested. It is probably by chance that MEAs #4-7 were not damaged as was sometimes observed with the excessively high hot-pressing pressure.

Most MEAs were performance tested at 100°C or 110°C before being heated and tested at higher temperatures. With all early MEAs, however, the performance decreased with increasing temperature. This was unexpected as both reaction kinetics and membrane conductivity increase proportionally with temperature and the phosphoric acid-doped PBI membrane was capable of operation at temperatures up to 200°C as specified by the manufacturer. The exact temperature at which the performance degradation began was uncertain, but it is certain that at 140°C the constant-current voltage of most MEAs decreased steadily over time. It was also observed that when MEAs were tested at 140°C immediately following testing at 100°C, performance loss was already evident.

It was initially assumed that membranes were developing pinholes and crossover leaks were forming during operation, decreasing the voltage output of the fuel cell. Every fuel cell showing performance degradation at high temperature was found to have crossover leaks after testing. Figure 22 shows the decrease in performance of MEA#5 over three consecutive trials, measured over 45 minutes.

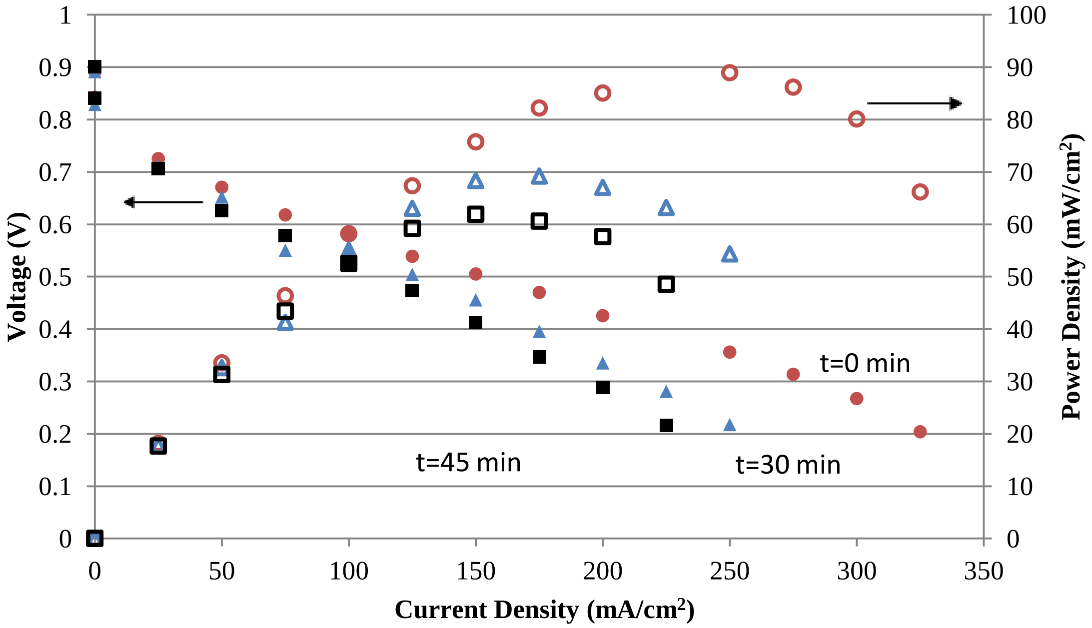

Figure 22: Performance degradation of MEA#5 over 3 consecutive trials at 140°C. Hydrogen and air flow rates were held constant at 200 mL/min. The fuel cell was operated at atmospheric pressure.

The data points in Figure 22 represent the average voltage measured over approximately 20 seconds at each current density, and not the equilibrium values of the system. In each case where this degradation was observed the voltage continued to decrease without ever reaching a steady state. Figure 22 therefore shows the performance of the MEA after a reasonable settling time and not their true steady state performance.

4.7 Improved Method for Membrane Electrode Assembly Fabrication

It became evident that there were problems with the initial method of fabricating the MEAs. The frequent damage to the electrodes during hot-pressing and the poor performance (relative to performance reported in the literature [46][47]) needed to be rectified. A number of researchers had reported that impregnating the electrode with phosphoric acid before hot-pressing caused a significant improvement in performance. Two approaches were used to include acid impregnation of the electrodes as part of the fabrication procedure: one using commercial PBI-impregnated Pt/carbon cloth electrodes (Danish Power Systems) that were subsequently doped with phosphoric acid (MEA#8) and the other using commercial untreated Pt/carbon paper electrodes (Electrochem) that were coated in PBI and doped with phosphoric acid (MEA#9). The performances of MEA#8 and MEA#9 are presented in Figure 23 and Figure 24 respectively. The hot pressing conditions for MEA#8 and MEA#9 are presented in Table 8.

It is important to recognize that MEAs #8 and #9 were hot-pressed at the intended pressure. The previously mentioned assumption was corrected and MEAs were hot-pressed at a pressure comparable to those which were used in recent studies by Cho *et al.* [39] and Li *et al.* [46]. Gas flowrates were set to 200 mL/min and the cells were operated at atmospheric pressure and tested on a Hydrogenics G60 fuel cell test station. Fuel cells were assembled using reinforced silicone gaskets. At the maximum current density the air and hydrogen stoichiometries were 3.3 and 15.6 respectively.

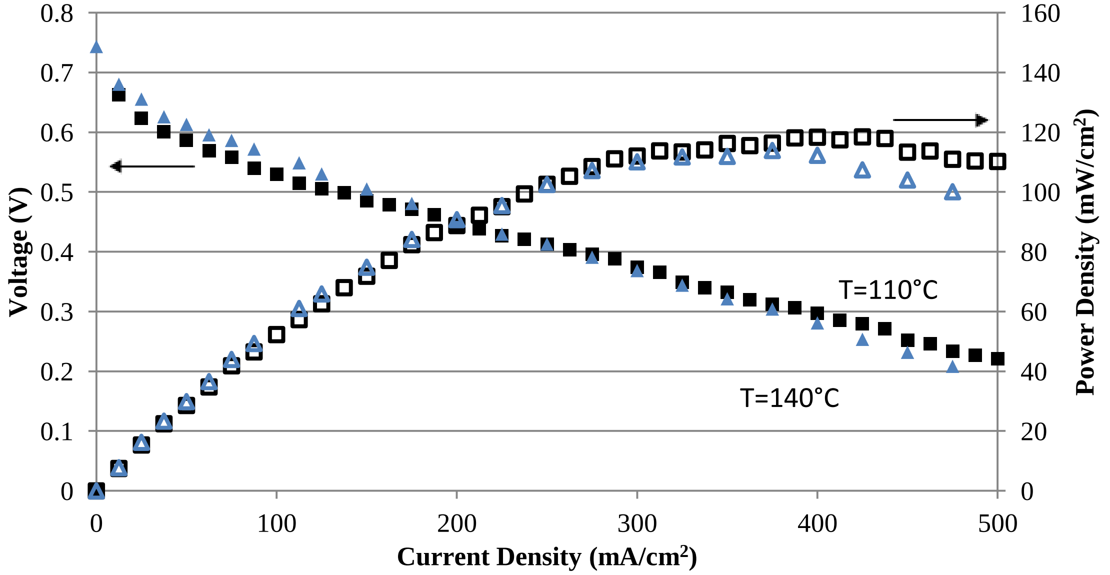

Figure 23: Performance of MEA#8 at 110°C and 140°C. Hydrogen and air flowrates were held constant at 200 mL/min. The fuel cell was operated at atmospheric pressure.

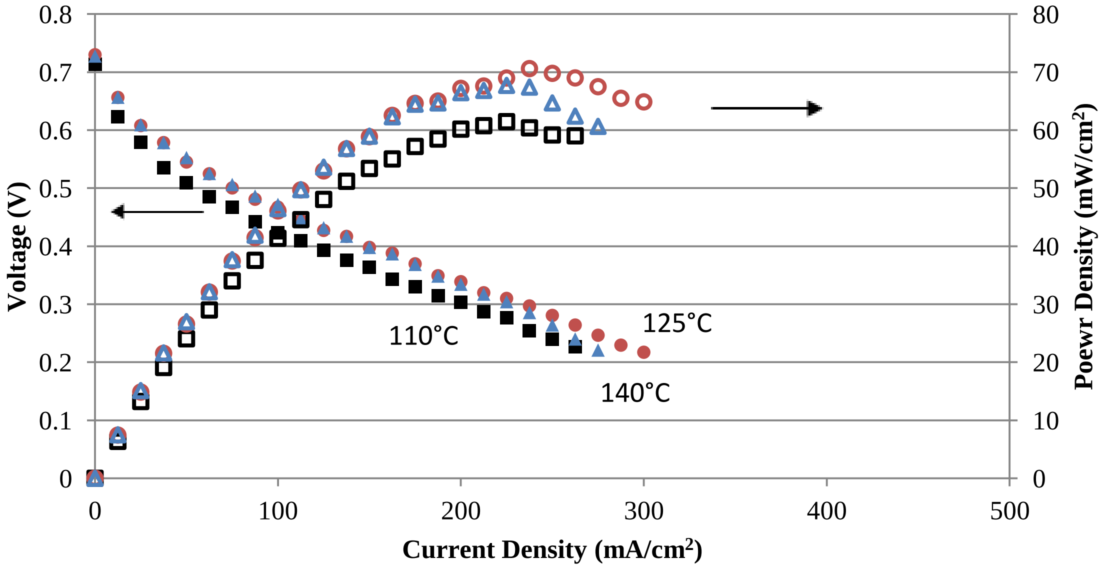

Figure 24: Performance of MEA#9 at 110°C, 125°C and 140°C. Hydrogen and air flowrates were held constant at 200 mL/min. The fuel cell was operated at atmospheric pressure.

Table 8: Maximum performance at 110°C, doping level and hot-press conditions for MEA#8 and MEA#9

	Doping Level (mol H_3PO_4/mol PBI)	Hot Press Time (min)	Hot Press Pressure (MPa)	Hot Press Temperature (°C)	Maximum Power Density (mW/cm^2)	Current Density at Maximum Power Density (mA/cm^2)
MEA#8	6.24	25	16.7	130	118	400
MEA#9	6.13	25	16.7	130	61.5	225

The performance of MEAs#8 and #9 was improved with respect to previously tested MEAs that had had no electrode modifications. Their performance, however, was not comparable to the performances of H_3PO_4-doped PBI fuel cells that have been reported in recent literature [47][60]. It was also not high enough to warrant testing in the TRFC system.

None of the MEAs in Figure 22, Figure 23 or Figure 24 showed improved performance when their operating temperature was raised above 100°C. As mentioned previously it was believed that pinholes were forming in the membranes during operation and crossover leaks were causing a voltage loss that progressively worsened as the leaks increased in size. Post-operation crossover leak testing validated this assumption in part, as crossover leaks were indeed present in all MEAs that had been tested at temperatures above 100°C. The cause of the pinhole formation was not understood. Post-testing examination of the MEAs and gaskets also showed that many of the gaskets appeared to be deteriorated where they had contacted the membrane.

The chemical and thermal stability of the silicone gasket material was investigated. A drop of 5M H_3PO_4 was placed on top of a piece of the gasket material and left in a 140°C oven overnight. The gasket visibly degraded while exposed to the acid in the oven. Upon removal from the oven the gasket had swelled, its texture had become gel-like and its mechanical strength had greatly decreased.

Teflon gaskets were used in the assembly of subsequent fuel cells at the suggestion of the MEA manufacturer. The Teflon gaskets showed no evidence of degradation in the fuel cell environment, and subsequently assembled fuel cells were successfully tested at temperatures in excess of 100°C.

4.8 H_2-Air Performance of Commercial Polybenzimidazole Membrane Electrode Assemblies

A fuel cell using a Dapozol ® G33 MEA (Danish Power Systems) was assembled using Teflon gaskets and performance tested. Figure 25 shows the performance of this MEA, which is labelled MEA#10, and the maximum performance is described in Table 9. Gas flow rates and back pressures were set to 200 mL/min and the cell was operated at atmospheric pressure and tested on a Hydrogenics G60 fuel cell test station. The fuel cell was assembled using Teflon gaskets. At 160°C the hydrogen and air stoichiometries at the maximum current density were 2 and 8.33.

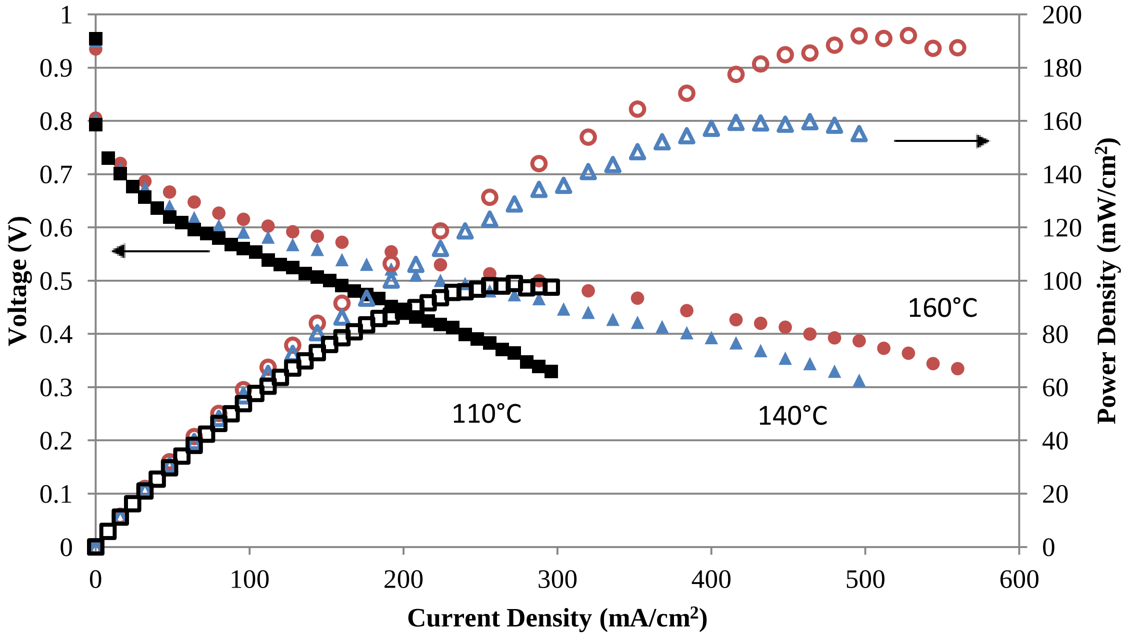

Figure 25: Performance of MEA#10 at various temperatures. Hydrogen and air flowrates were held constant at 200 mL/min. The fuel cell was operated at atmospheric pressure.

Table 9: Maximum performance of MEA#10 at various temperatures.

Temperature (°C)	Maximum Power Density (mW/cm^2)	Current Density at Maximum Power Density (mA/cm^2)
110	97	280
140	159	448
160	192	528

As seen in Figure 25 the performance of the commercial MEA increased as the temperature was raised; it was assumed that the use of Teflon gaskets allowed the MEA to be heated above 100°C without crossover leaks developing. Although the performance of the commercial MEA was not substantially better than that observed in MEAs #4, #6 and #7 (Figure 21), it was commercially obtained and offered the possibility of replicate trials. The achieved performance of MEA#10 at temperatures of 140°C and 160°C exceeded the performance threshold that had been previously described. A second commercial MEA (MEA#11) was therefore assembled and tested on the

Arbin BT2000 system under H_2-air conditions; the performance of this MEA is presented in Figure 26. Hydrogen and air flow rates were set to 900 mL/min and 150 mL/min respectively and the fuel cell was operated at atmospheric pressure at a temperature of 160°C. These flow rates were selected to meet stoichiometric flow ratios of 2.5 and 3 for the fuel and oxidant respectively at a maximum current draw of approximately 1.2 A/cm2.

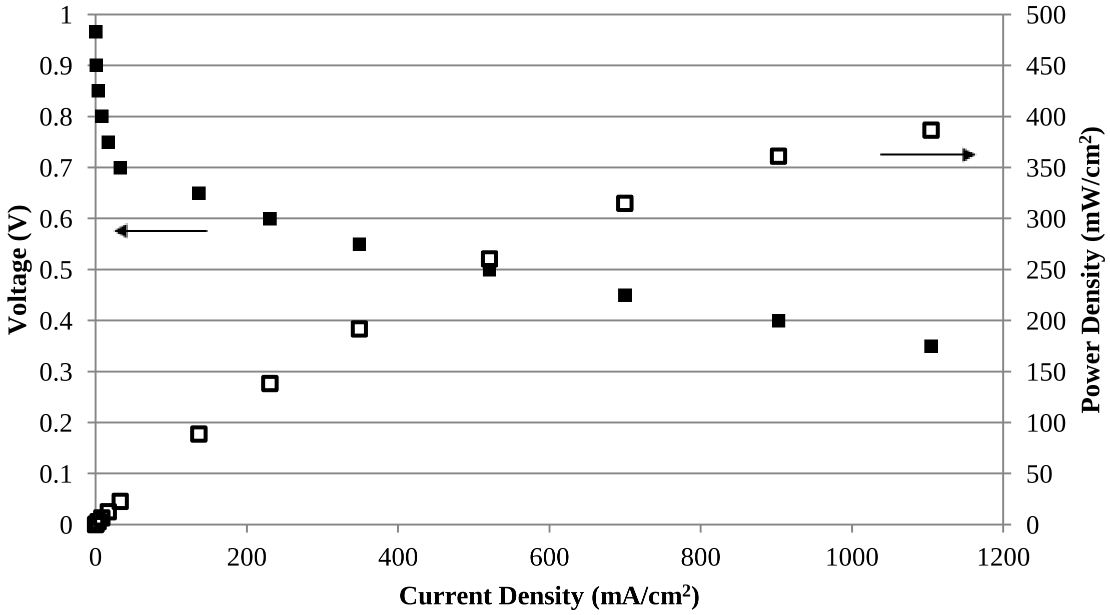

Figure 26: Performance of MEA#11 at 160°C. Hydrogen and air flowrates were held constant at 900 mL/min and 150 mL/min respectively. The fuel cell was operated at atmospheric pressure.

MEA#11 showed the highest performance of any MEA tested during this experimental work, with a maximum power density and current density of 390 mW/cm^2 and 1100 mA/cm^2 respectively. The maximum flow rate of air was limited to approximately 1000 mL/min by the mass flow controller. Higher current densities could therefore not be drawn without operating at an air stoichiometric ratio of less than 3, and the trial was stopped shortly before a maximum power density was observed. An improvement in performance was observed compared to that of the MEA#10, in which the air flow stoichiometry was less than 2. It is believe that the increased amount of oxygen molecules arriving at the cathode helped to overcome sluggish oxygen reduction reaction kinetics, which increased the fuel cell performance.

A large drop in fuel cell voltage at low current densities was observed for most of the MEAs that were tested in this work. Voltage efficiency decreases in this region of a polarization curve are attributed to activation kinetics. These voltage drops are likely due to the manufacturing methods of the electrodes that were used; however this was not studied in detail.

4.9 *Ex-situ* Membrane Resistance Studies of Polybenzimidazole in Propiophenone

The membrane resistance of PBI in propiophenone was studied using *ex-situ* electrochemical impedance spectroscopy [52]. Membrane samples of various phosphoric acid doping levels were immersed in propiophenone and then characterized using electrochemical impedance spectroscopy.

It was observed that the impedance of each membrane sample increased significantly over the testing period. To minimize the uncertainty in the measurements repeated trials were conducted over several hours for each membrane sample to observe the change in impedance, and average membrane conductivity and resistance values were determined. Typically each impedance spectrum was recorded 30-60 minutes after the previous spectrum and approximately 20 consecutive spectra were obtained for each sample. Figure 27 presents a Nyquist plot that shows the impedance spectra for 4 consecutive trials on a PBI membrane with an acid doping level of 4.88 mol H_3PO_4/mol of repeat unit PBI that was immersed in propiophenone at 120°C. A single semi-circular response and significant amounts of noise at low frequencies were observed in every trial.

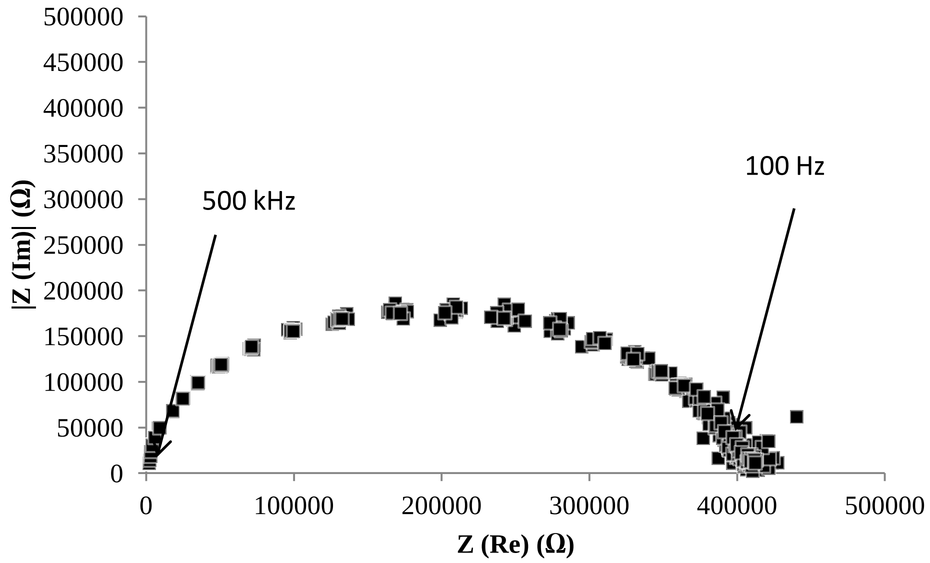

Figure 27: Nyquist plot showing the impedance spectra of a phosphoric acid doped PBI membrane (DL: 4.88) immersed in propiophenone at 120°C

Figure 28 shows the high frequency impedance of a PBI membrane with an acid doping level of 2.18 mol H_3PO_4/ mol PBI. Analysis showed that the membrane resistance increased with increasing temperature. Two possible explanations of this observation are that: 1) the presence of the ketone caused the dehydrogenation of phosphoric acid to pyrophosphoric acid at a lower temperature than is expected for hydrogen-air fuel cell operation. Pyrophosphoric acid has different ion transfer mechanisms than phosphoric acid and could lead to lower membrane conductivity [61]. 2) The propiophenone leached out the phosphoric acid from the membrane. It is possible that at higher temperatures propiophenone could pull acid from the membrane more effectively, decreasing the membrane conductivity.

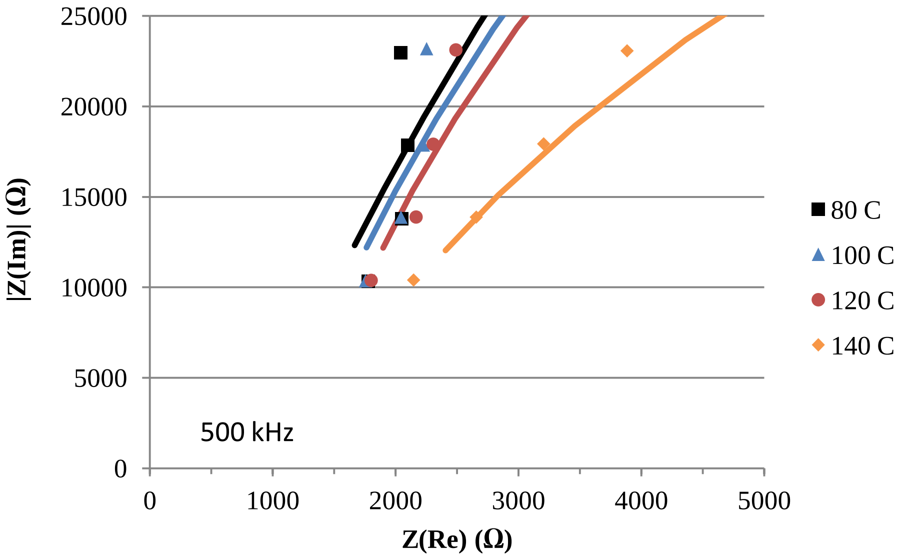

Figure 28: High frequency impedance data of PBI membrane with an acid DL of 2.18. Membrane was immersed in propiophenone and tested at various bath temperatures.

Calculated average membrane resistance and conductivity values are compiled in Table 10 for membrane doping levels of 2.81 and 4.88 mol H_3PO_4/ repeat unit PBI respectively. The test frequencies were not high enough to observe the actual real axis intercept; the reported membrane resistances were therefore extrapolated using the ZFit analysis tool. There is an anomalous point in the data for the 120°C test of PBI membrane with DL: 4.88; the values do not follow the observed trend and are assumed to be incorrect. The measured conductivities of the commercial membranes studied in this work are much higher than typically reported fuel cell membrane conductivities. These values are potentially characteristic of the conductivity of acid-doped PBI membrane immersed in propiophenone, however literature to validate this assumption does not exist. The results do, however, illustrate that the conductivity of the membranes increases with temperature, as is expected.

Table 10: Calculated average in-plane resistance and conductivity of PBI membranes at various doping levels and temperatures

	DL: 2.81mol H_3PO_4/ repeat unit PBI		DL: 4.88 mol H_3PO_4/ repeat unit PBI	
Temperature (°C)	Average Resistance (Ω)	Average Conductivity (S/cm)	Average Resistance (Ω)	Average Conductivity (S/cm)
80	838.9	0.275	270.9	0.852
100	1048.6	0.220	324.8	0.710
120	1232.2	0.187	1685.2	0.137
140	1277.5	0.181	964.8	0.239

In many trials numerical analysis of results was not possible due to severe degradation of the membrane during testing. Membrane discoloration was observed, and upon removal from the propiophenone bath they were found to be very brittle. It was also noted that pieces of the shattered brittle membrane regained their pliability after a few days of sitting exposed to air in a fume cupboard. Figure 29 shows an image of a highly doped PBI membrane that degraded quickly upon immersion in a heated propiophenone bath.

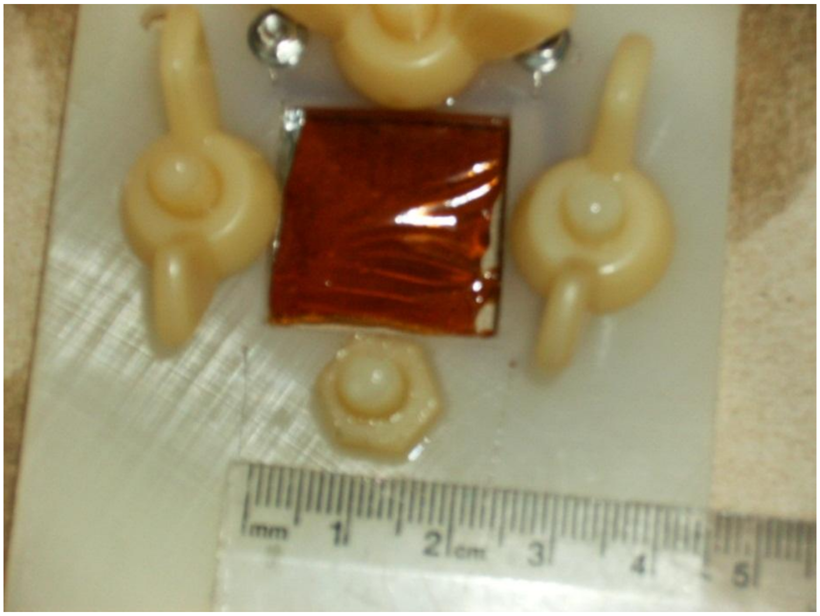

Figure 29: Degradation of phosphoric acid-doped PBI membrane (DL: 8.64) after immersion in propiophenone for a few hours at 80°C

Along with the discoloration and developing brittleness of the membrane, discoloration was observed in the propiophenone and Nylon support. The propiophenone in the bath was used for multiple trials, and it was observed that the color changed from colorless through pale yellow to orange and finally brown. This gradual color shift implied that propiophenone contamination was occurring progressively. Both gas chromatography and mass spectrometry were used to determine the nature of the impurities developing in the propiophenone, but although contaminants were observed they could not be identified. The conductivity of the discolored propiophenone solution was also compared to that of fresh propiophenone. It was found that while the fresh propiophenone had a conductivity of 0 S/cm, the discolored propiophenone had a conductivity of 0.7 µS/cm. It is likely that leached phosphoric acid was the cause of the increased propiophenone conductivity.

It was hypothesized that low molecular weight PBI and/or phosphoric acid was leaching from the membrane over time and contaminating the propiophenone. It was also suggested that phosphoric acid could have been catalyzing an aldol condensation reaction between two propiophenone molecules. These findings are important with respect to the TRFC because decreases in the membrane durability in the presence of propiophenone will affect the operation of the system. The progressive contamination of the propiophenone is also of concern due to the recycling of fluid that will take place in the TRFC.

4.10 Thermally Regenerative Fuel Cell Performance of Commercial Polybenzimidazole Membrane Electrode Assemblies

MEA#11 was subsequently used to test the performance of the hydrogenation reaction. The fuel cell was assembled using Teflon gaskets. Propiophenone was fed to the cathode at 0.01 mL/min and hydrogen was fed to the anode at 50 mL/min. The fuel cell was operated at atmospheric pressure at a temperature of 160°C. Initial testing using the Arbin BT-2000 test system's electronic load to generate polarization curves showed that the system was incapable of accurately drawing the low currents required to measure the performance of the TRFC.

A series of passive resistors was connected across the fuel cell to impose a steady load and generate a polarization curve at lower current densities than the Arbin system could provide. The resistors were connected across the fuel cell and voltage was monitored using the Arbin system. Assuming that the resistance of the membrane and fuel cell hardware was negligible Ohm's law was used to calculate the current passing through the resistor. The polarization curve does not have many data points beyond the maximum power density because appropriately sized resistors were not available. The generation of TRFC hydrogenation polarization curves required long experiment times because of the time required for the manual switching of each resistor as well as the long voltage stabilization times that were required at each new current density. The measured performance of the TRFC hydrogenation reaction using MEA#11 is shown in Figure 30.

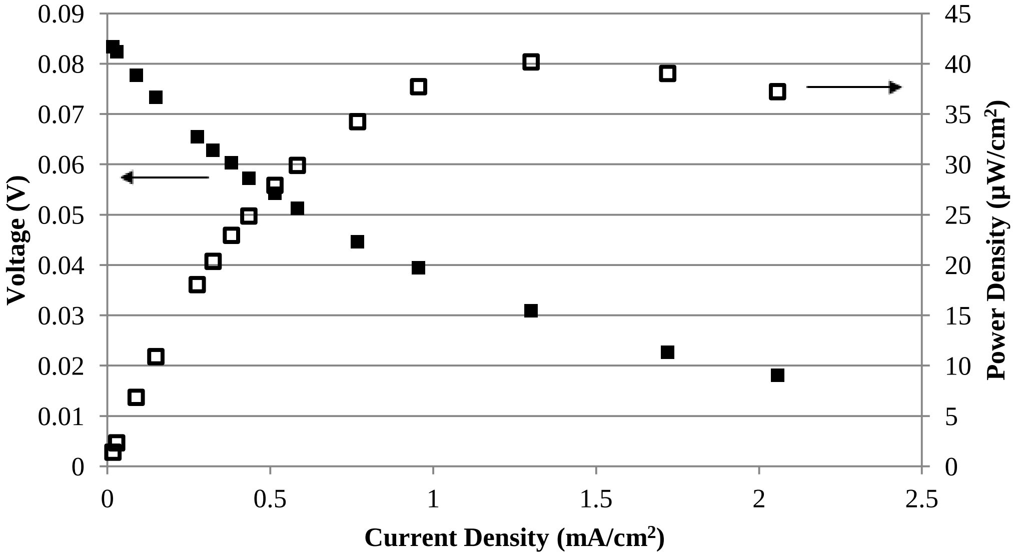

Figure 30: TRFC hydrogenation performance of MEA#11 at 160°C. Hydrogen and propiophenone flow rates were held constant at 50 ml/min and 0.01 mL/min respectively. The fuel cell was operated at atmospheric pressure.

Using passive resistors to limit the current through the TRFC a maximum power density of 40.2 μW/cm^2 was observed at a current density of 1.32 mA/cm^2. This measured performance is comparable but lower than the performances observed in the various gas phase TRFCs described in the literature review [1][29], however, it must be noted that the electrodes used in this work contain commercial platinum catalysts and no optimization has been attempted. In Chaurasia *et al.*'s [1] work it was observed that Pt catalysts were inferior to Pt/Ru composite catalysts, with a 300% increase in maximum power density observed when using the composite catalyst system. It is likely that a more suitable catalyst exists for the hydrogenation of propiophenone to 1-phenyl-1-propanol, but that it has not yet been located. It is also important to note that the total catalyst loading for the commercial electrodes used in this work was only 1.4 mg/cm^2, whereas the catalyst loadings reported in the literature ranged anywhere from 19 to 41 mg/cm^2, and were possibly even higher as they were not reported in some cases. The open circuit voltage of 98 mV observed during the TRFC hydrogenation is higher than the thermodynamically predicted cell voltage of 24.8 mV at 160°C.

After TRFC testing the fuel cell was disassembled and the MEA was examined for signs of degradation caused by the high temperature propiophenone. It was observed that propiophenone had crossed from the cathode to the anode during operation. Figure 31 and Figure 32 respectively show the anode and cathode-side membrane electrode assembly surfaces of MEA#11 after TRFC operation.

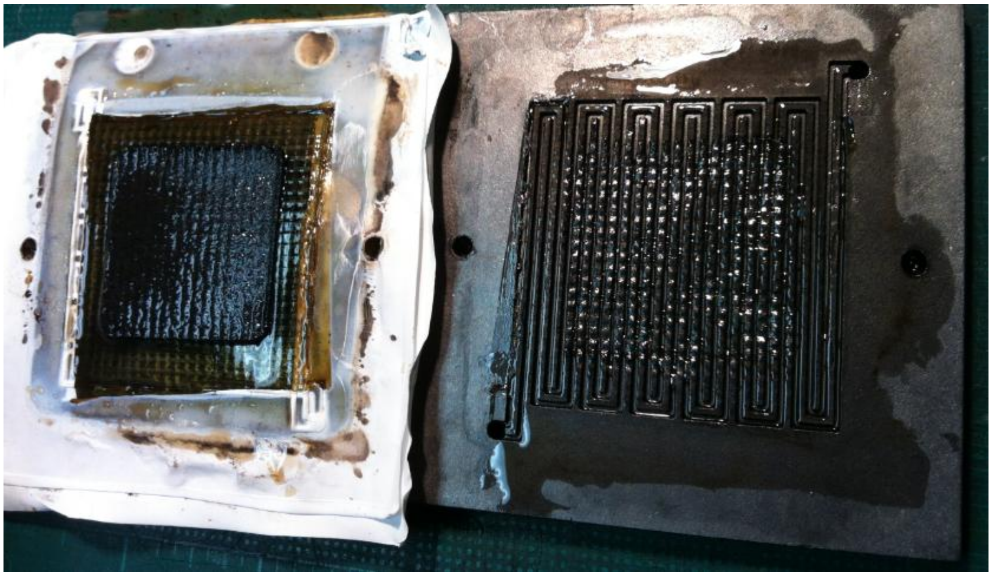

Figure 31: Anode-side membrane electrode assembly of MEA#11 after TRFC testing

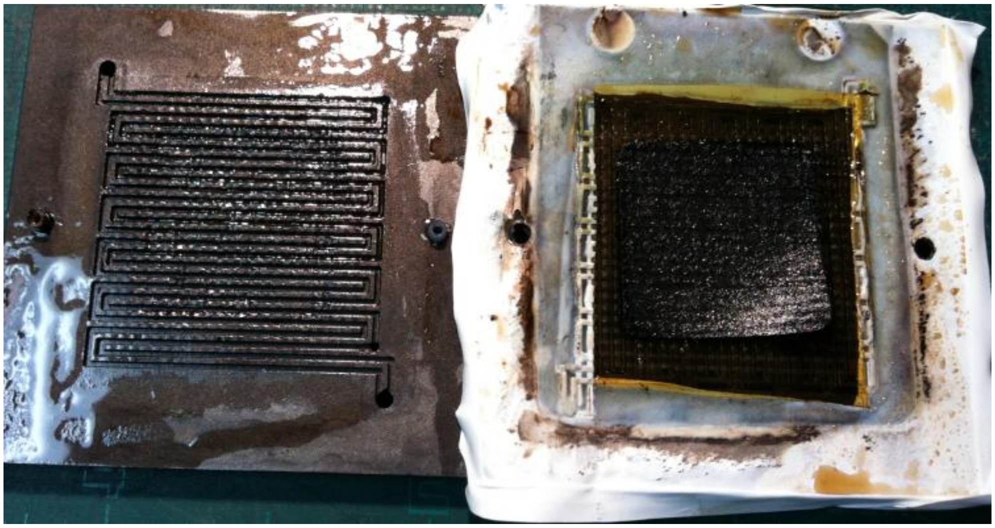

Figure 32: Cathode-side membrane electrode assembly of MEA#11 after TRFC testing

Both the anode and cathode electrodes and flow field plates of MEA#11 were visibly soaked with propiophenone in post-cell operation observation. It is unknown whether the propiophenone was able to penetrate through the membrane at elevated temperatures, however, previous testing had shown that this penetration did not occur at room temperature.

It can be seen in both Figure 31 and Figure 32 that the Teflon gaskets degraded in the TRFC during operation, turning a brown color and becoming transparent at the gasket-membrane interface. It is unknown whether this affected the properties of the gasket, or whether the gaskets were the cause of the observed propiophenone crossover.

A second commercial PBI MEA from the same provider was assembled and used to test the performance of the TRFC hydrogenation reaction (MEA#12). The fuel cell was assembled using Teflon gaskets. All operating conditions remained the same, except that the propiophenone flowrate was increased and was set to 0.01 mL/min (ten times larger than the propiophenone flow rate used during the testing of MEA#11). Fuel cell and propiophenone inlet temperatures were set to 160°C and hydrogen flow was set to 50 mL/min. The fuel cell was operated at atmospheric pressure on the Arbin BT2000 system. Current flow through the cell was limited by passive resistors. Figure 33 shows the hydrogenation performance of MEA#12 under TRFC conditions.

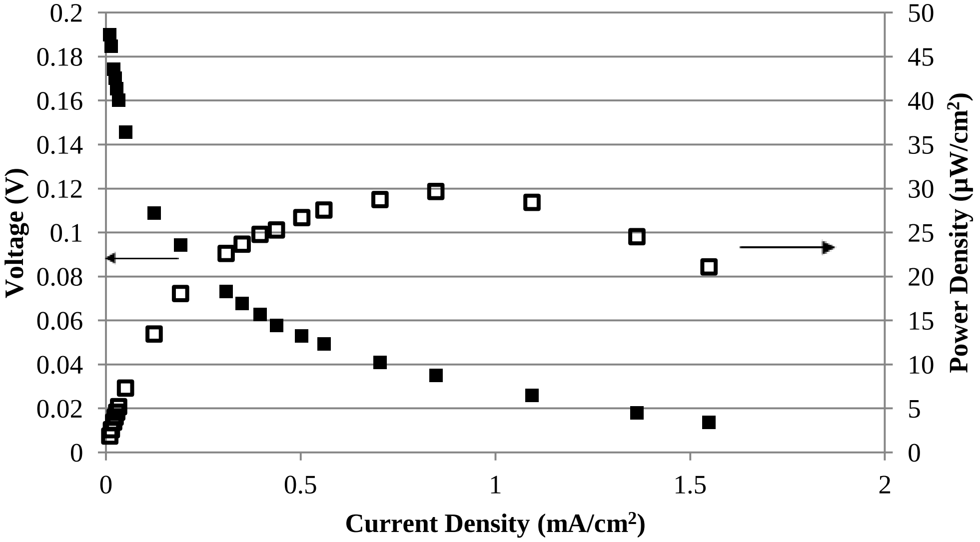

Figure 33: TRFC Hydrogenation Performance of MEA#12 at 160°C. Hydrogen and propiophenone flowrates were held constant 50 mL/min and 0.1 mL/min respectively. The fuel cell was operated at atmospheric pressure.

MEA#12 displayed a stable open circuit voltage of approximately 193 mV, nearly twice as high as the open circuit voltage displayed by MEA#11 under very similar conditions. In spite of the higher open circuit voltage the maximum power density of MEA#12 was lower than that of MEA#11 (30 µW/cm^2 as compared to 40 µW/cm^2 respectively). Examination of MEA#12 after TRFC operation did not show evidence of propiophenone crossover, as can be seen in Figure 34 and Figure 35. Propiophenone was observed on the cathode, as expected, but there was no evidence of propiophenone at the anode of the fuel cell.

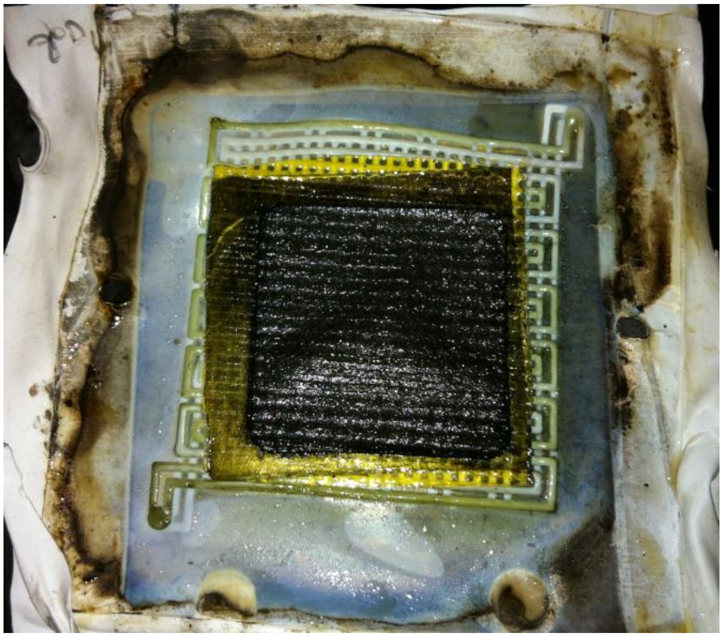

Figure 34: Cathode-side membrane electrode assembly of MEA#12 after TRFC testing

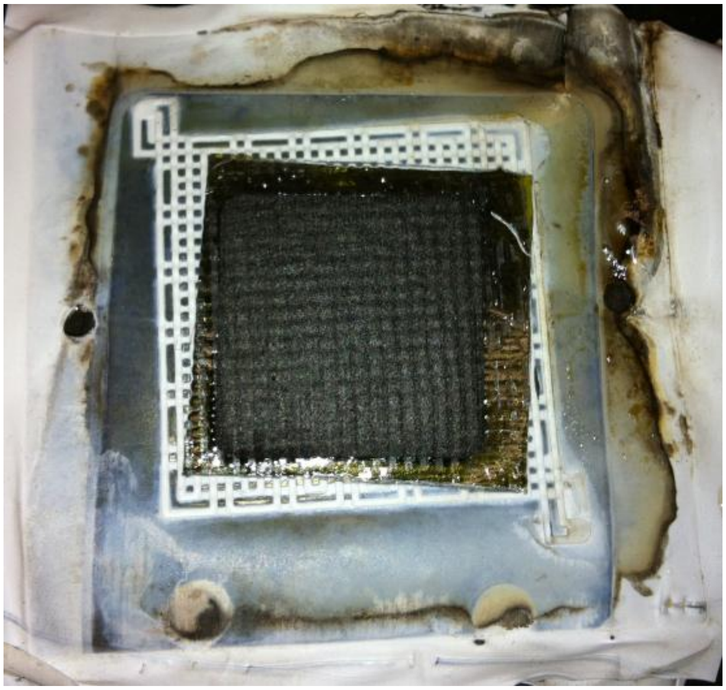

Figure 35: Anode-side membrane electrode assembly of MEA#12 after TRFC testing

MEA#12 was one of the first MEAs that was tested under TRFC conditions, and to get a feel for the system the MEA was tested repeatedly, and consequently left assembled in the fuel cell exposed to propiophenone for approximately 2 weeks. Over this period MEA#12 was heated from room temperature three times and performance tested at 160°C. Discoloration of the cathode-side gasket is evident in Figure 34. It is unknown if this discoloration is due to the long exposure to the propiophenone or the combination of heat and organic liquid, but the color change likely indicates damage to some part of the fuel cell assembly.

Only two trials were used to test the hydrogenation performance of the TRFC system, and due to the different performance results more trials are required before any conclusions on the TRFC performance can be made.

4.11 Gas Chromatograph Analysis of Thermally Regenerative Fuel Cell Cathode Liquid

A gas chromatograph was used to analyze the hydrogenation reaction taking place within the TRFC. The propiophenone requirement of the hydrogenation reaction was very small and collecting the propiophenone effluent from the TRFC during normal operation would likely result in the analysis of very small volumes of hydrogenated compound, which would potentially have been undetectable. To increase the proportion of hydrogenation product in the sample, the cathode was sealed and the HPLC pump turned off so that hydrogenation only occurred on the volume of propiophenone sitting within the flowfield plates. A 1Ω resistor was connected across the cell to allow current to flow, and the voltage was measured to allow later estimation of the current that had flowed, and therefore the approximately amount of hydrogenation that had occurred. The cell was held at 160°C for approximately 16 hours, and hydrogen was passed through the anode at 50 mL/min. The recorded voltage of the fuel cell and the calculated total hydrogenation amount are presented in Figure 36.

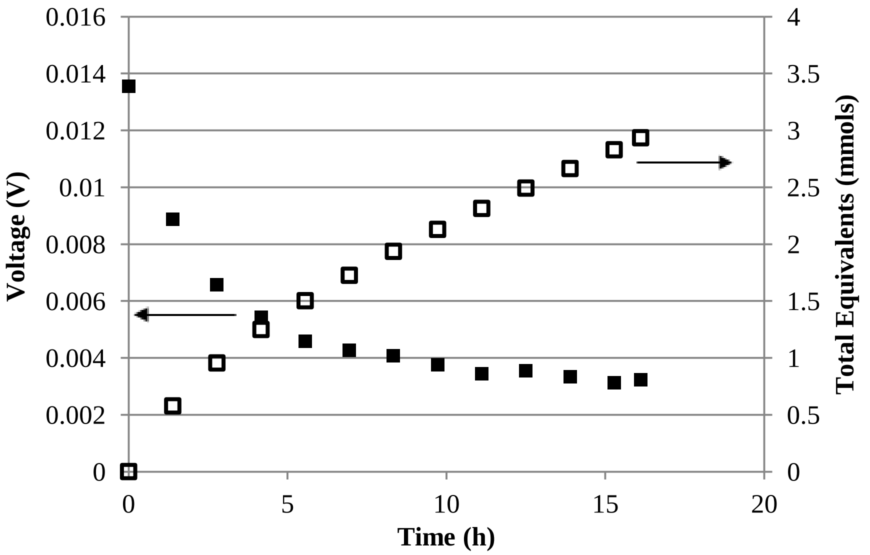

Figure 36: Recorded fuel cell voltage and total equivalents during 16h closed-cell operation

The voltage of the hydrogenation reaction was seen to decrease progressively over the 16 hour experimental period. This voltage change was expected due to the anticipated changes in the cathode reactant composition.

The total current that had passed across the circuit was calculated based on the voltage and resistance of the cell using Ohm’s law. Using an estimate of the flowfield plate volume, the calculated total current flow indicated a hydrogenation conversion of 16% of the total cathode flowfield plate volume (or 44% of the volume directly adjacent to the electrode), assuming 100% reaction selectivity. The reaction volume was collected and analyzed using a gas chromatograph to examine the selectivity of the hydrogenation. The GC results are presented in Figure 37.

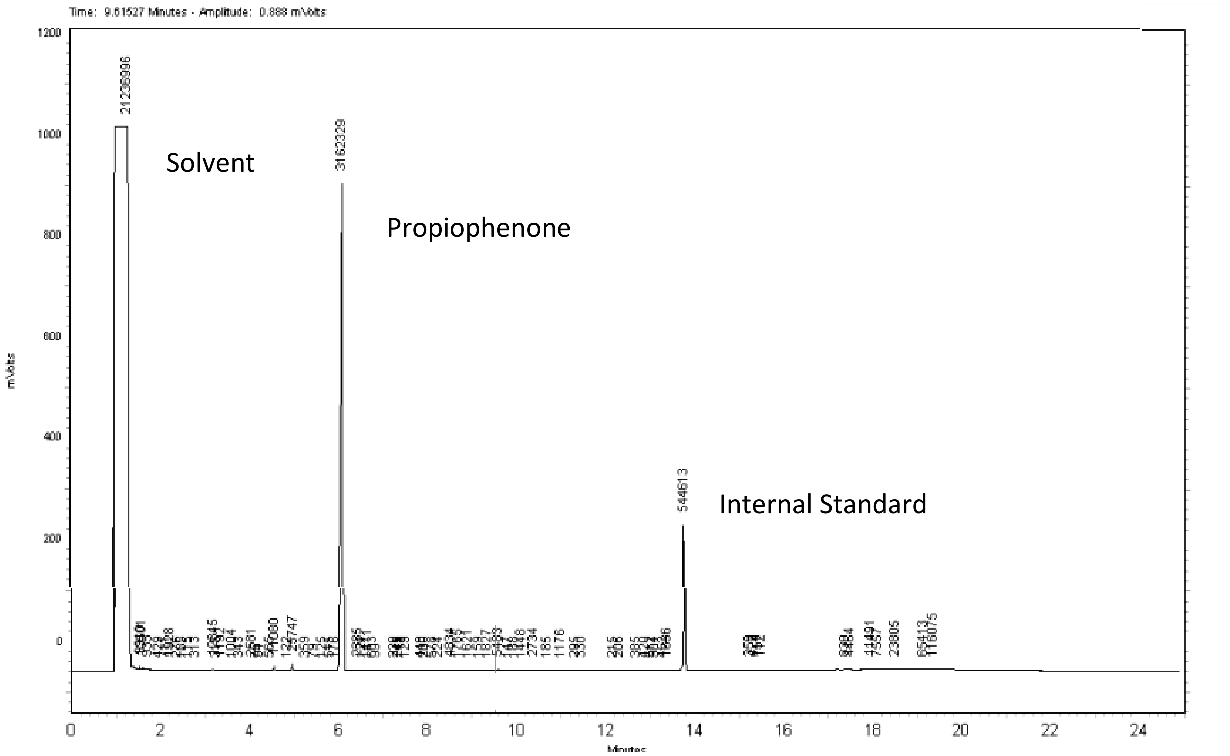

Figure 37: Gas chromatogram of TRFC cathode fluid after 16h of operation

To within the limits of detection, the gas chromatograph did not indicate any 1-phenyl-1-propanol was present in the sample from the TRFC cathode chamber. Aside from the large solvent and internal standard peaks at 1.3 and 14 minutes respectively only one major peak was seen in the sample, although two smaller peaks were observed between 4 and 5 minutes. Previous sample trials of pure propiophenone and 1-phenyl-1-propanol had determined that propiophenone came off of the column at approximately 6.1 minutes and 1-phenyl-1-propanol came off at approximately 6.4 minutes. Mass spectrometer results later showed that the molecular mass of the compound with a retention time of 6 minutes had a molecular weight of 134 g/mol, confirming that it was propiophenone, as the molecular weight of 1-phenyl-1-propanol is 136 g/mol.

Because the current that passed through the TRFC over the 16 hour reaction time was sufficient to hydrogenate approximately 15% of the total flowfield volume it was surprising that no hydrogenation products were observed. It is unlikely that oxygen (either dissolved in the propiophenone or entering the cathode through a leak) was reduced to produce the observed current because of the large volume of air that would be required to produce the observed current; approximately 34 mL of oxygen or close to 162 mL of air at 298K and atmospheric pressure would have been required in the fuel cell. The volume of the flow field plate was approximately 1.5 mL which means that if air or oxygen was present in the cell during TRFC operation, it had to have leaked in during operation. The average rate of this leak would have to have been approximately 0.03 mL/min of oxygen or 0.16 mL/min of air, but this is also unlikely given the small pressure gradient that air would have to push against to enter the cell through a leak.

Another possibility is that the hydrogenation reaction did occur, but when the cathode of the TRFC was drained for analysis, the product remained inside the gas diffusion layer of the electrode where the reaction had taken place. If the hydrogenation reaction produced the observed current than the volume of 1-phenyl-1-propanol product would only be 0.2 mL, and this amount of liquid could have remained within the carbon cloth electrode. The MEA was retained after testing and a thorough methanol rinse of the MEA (focusing on the gas diffusion electrodes) followed by GC testing again failed to detect any presence of the expected 1-phenyl-1-propanol. It has been noted by other researchers that simple alcohols can react in phosphoric acid-doped PBI fuel cells to produce organic phosphate esters [62]. It is possible that 1-phenyl-1-propanol was not detected by the GC because it had already reacted to form an organic phosphate ester, and that the molecule was insoluble in the methanol rinse and therefore not analyzed by the GC. Given the observed current draw and the lack of other plausible explanations, it is suspected that the expected hydrogenation of propiophenone to 1-phenyl-1-propanol occurred, but was simply not detected.

This would also explain the higher than thermodynamically predicted cell voltage that was observed. The Gibb's free energy change of the hydrogenation reaction is directly related to the cell potential. The electrochemical production of a tri-aryl phosphate molecule would result in a large negative entropy of reaction, which would lead to an increased Gibb's free energy of reaction and a consequently larger cell voltage.

Summary of Main Findings

1. The thermally regenerative fuel cell operated successfully. Current was drawn from the system and a polarization plot was created, however, gas chromatograph and mass

spectrometer analysis of the cathode chamber fluid were not able to detect the presence of the hydrogenated compound.

2. Impedance spectroscopy testing showed that phosphoric acid-doped polybenzimidazole is severely damaged by propiophenone at high temperatures. Long term operation of the system as currently configured is likely not possible.
3. An acceptable method for fabricating in-house MEAs was developed. Although the fabricated MEAs do not compare favourably with commercial MEAs, optimization of hot-pressing conditions and electrode polymer content and acid doping could increase their performance.

Chapter 5 Conclusions and Recommendations

5.1 Conclusions

Software modelling results suggested that the equilibrium conversion of the dehydrogenation reaction would be low unless the temperature of the reactor is held close to the boiling point of propiophenone and 1-phenyl-1-propanol.

A system was designed and built to test the performance of a thermally regenerative fuel cell's hydrogenation reaction. The test system enabled control of fuel and oxidant flowrates and temperatures and precise control and monitoring of the current and voltage of fuel cells in both hydrogen-air and organic liquid-based thermally regenerative fuel cell operation. The system will be used by current and future members of the TRFC research group to test newly developed hydrogenation catalysts and electrode formulations.

The hydrogen-air performance of high temperature phosphoric acid-doped polybenzimidazole membrane electrode assemblies was determined using the new test system. At a temperature of 160°C and at atmospheric pressure with hydrogen and air flowrates of 150 mL/min and 900 mL/min respectively the maximum power density of the cell was 387 mW/cm^2 at a current density of 1.1 A/cm^2.

The compatibility of polybenzimidazole membranes with respect to propiophenone was analyzed using electrochemical impedance spectroscopy. Membranes durability decreased rapidly upon immersion in propiophenone at elevated temperatures. At high acid doping levels (approximately 10 mol H_3PO_4/repeat unit PBI) membranes partially dissolved, and at lower doping levels (between 2 and 6 mol H_3PO_4/ repeat unit PBI) membranes became brittle, shattering with minimal applied force. It was furthermore observed that the propiophenone bath gradually changed from colorless to a dark yellow/orange color over the course of testing. The Nylon membrane support structure also turned from white to brown.

The conductivity of the propiophenone bath was measured at 0.7 µS/cm after contamination compared to 0 µS/cm for a fresh sample. This increase in conductivity is attributed to the leaching of phosphoric acid from the membranes into solution.

In spite of the indications of the materials' incompatibility, commercial phosphoric acid-doped PBI MEAs were used to evaluate the hydrogenation performance of the TRFC as they were the only readily available MEA that could operate in a non-aqueous fuel cell at this temperature. At 160°C and atmospheric pressure with hydrogen and propiophenone flowrates of 50 mL/min and 0.01 mL/min respectively, the maximum power density was 40 µW/cm^2 at a current density of 1.3 mA/cm^2. This is lower but comparable to the performance of previously described literature TRFC systems using optimized electrode catalyst loadings [1][29].

Propiophenone was found on both sides of the membrane following TRFC operation. This may have been due to inadequate sealing by the Teflon gaskets, but may also be the result of propiophenone diffusing through the PBI membrane.

5.2 Recommendations

Though the test system that was built is completely functional and performed well during TRFC testing, certain improvements could be made. The addition of pressure gauges and check valves up and downstream of the fuel cell would enable hydrogenation performance analysis at elevated pressures, which is currently not possible. The current method of manually applying and detaching passive resistors across the cell could be streamlined by incorporating those same resistors into a manual load box.

Further trials would reduce the uncertainty of the reported maximum performance, and would determine the performance at temperatures and flowrates other than those examined in this work.

The choice of both membrane and working fluid should be revaluated, as long term operation using the current selections does not seem possible given the membrane acid-leaching, membrane deterioration and working fluid contamination that were observed.

If the working fluids are unchanged in future iterations of the TRFC system, it is possible that a gasket material other than Teflon will be necessary, as the Teflon gaskets that were used in this work were visibly degraded during operation.

Further optimization of the catalyst system is required. Chaurasia *et al.* [1] found that in their acetone/2-propanol TRFC Pt/Ru composite electrodes substantially outperformed monometallic Pt electrodes with identical catalyst loadings. Electrode optimization was not attempted for this study, but its implementation is strongly recommended.

References

[1] P. Chaurasia, Y. Ando and T. Tanaka, "Regenerative fuel cell with chemical reactions," *Energy conversion and management,* pp. 611-628, 2003.

[2] "Energy Flow," 2011. [Online]. Available: https://flowcharts.llnl.gov/index.html. [Accessed September 2012].

[3] J. Smith, H. Van Ness and M. Abbott, Introduction to Chemical Engineering Thermodynamics, McGraw-Hill, 2004.

[4] "Found Energy," 2012. [Online]. Available: www.foundenergy.ca.

[5] R. Dervisoglu, "Fuel Cell," May 2012. [Online]. Available: http://en.wikipedia.org/wiki/Fuel_cell.

[6] J. Larminie and A. Dicks, Fuel cell systems explained, West Sussex: Wiley, 2003.

[7] E. Winder, A. Ellis and G. Lisensky, "Thermoelectric Devices: Solid state refrigerators and electric generators in the classroom," *Journal of Chemical Education,* pp. 940-946, 1996.

[8] A. Van Herwaarden and P. Sarro, "Thermal sensors based on the Seebeck effect," *Sensors and Actuators,* pp. 341-346, 1986.

[9] F. DiSalvo, "Thermoelectric cooling and power generation," *Science,* pp. 703-706, 1999.

[10] H. Liebhafsky, "Regenerative electrochemical systems: An introduction," in *Regenerative EMF Cells*, Washington, D.C., American Chemical Society, 1967, pp. 1-10.

[11] H. Liebhafsky, "The fuel cell and the carnot cycle," *Journal of the Electrochemical Society,* pp. 1068-1071, 1959.

[12] J. Angus, "Continuous gas concentration cells as thermally regenerative galvanic cells," in *Regenerative EMF cells*, American Chemical Society, 1967, pp. 11-16.

[13] I. Groce and R. Oldenkamp, "Development of a thermally regenerative sodium-mercury galvanic system. Part II. Design, construction and testing of a thermally regenerative sodium-mercury galvanic cell," in *Regenerative EMF cells*, American Chemical Society, 1967, pp. 43-52.

[14] R. Oldenkamp and H. Recht, "Development of a thermally regenerative sodium-mercury gavanic cell. Part III. Performance analysis for a nuclear-powered, thermally regenerative sodium-mercury galvanic system," in *Regenerative EMF cells*, American Chemical Society, 1967, pp. 53-61.

[15] B. Agruss and H. Karas, "The thermally regenerative liquid metal concentration cell," in *Regenerative EMF cells*, American Chemical Society, 1967, pp. 62-81.

[16] Y. Ando, T. Doi, T. Takashima and T. Tanaka, "Proposal and fundamental analysis of thermally regenerative fuel cell utilizing waste heat," in *Proceedings of the 32nd annual intersociety energy*

conversion engineering conference, Honolulu, 1997.

[17] A. Carrier, *The transportation and transformation of energy through reversible hydrogenation,* Ph.D. Disseration, Department of Chemistry, Queen's University, Kingston, 2011.

[18] D. Dean, *Hydrogen fuel technologies for vehicular transportation,* Ph.D. Dissertation, Department of Chemistry, Queen's University, Kingston, 2012.

[19] M. Bradfield, "Improving alternator efficiency measurably reduces fuel costs," Remy, Inc., 2008.

[20] C. Cooper, F. Kamakate, T. Reinhart, M. Kromer and R. Wilson, "Reducing heavy-duty long haul combination truck fuel consumption and CO2 emission," 2009.

[21] L. Heredy, M. Iverson, G. Ulrich and H. Recht, "Development of a thermally regenerative sodium-mercury galvanic system. Part I. Electrochemical and chemical behavior of sodium-mercury galvanic cells," in *Regenerative EMF cells*, American Chemical Society, 1967, pp. 30-42.

[22] D. Basiulis, F. Ludwig, J. McHardy and A. Kindler, "Thermally regenerative fuel cells," Office of naval research, El Segundo, 1991.

[23] J. Morehouse, "Thermally regenerative hydrogen/oxygen thermally regenerative fuel cell cycles," *Journal of solar energy engineering,* pp. 107-112, 1988.

[24] Y. Saito, K. Matsuo and Y. Yatabe, "Catalyst-assisted utilization of waste heat," 1987.

[25] Y. Ando and T. Tanaka, "A study on the solar thermal cell - the influence of proton conductivity in a polymer electrolyte membrane and electrical conductivity on the output of solar thermal cell," in *Energy Conversion Engineering Conference*, Washington, D.C., 2002.

[26] Y. Ando, T. Tanaka, T. Doi and T. Takashima, "A study on a thermally regenerative fuel cell utilizing low-temperature thermal energy," *Energy Conversion and Management,* pp. 1807-1816, 2001.

[27] Y. Ando and T. Tanaka, "A study on the solar thermal cell - the influence of proton conductivity in a polymer electrolyte membrane and electrical conductivity on the output of the solar thermal cell," in *Energy Conversion Engineering Conference*, Washington, D.C., 2002.

[28] Y. Ando, T. Tanaka and M. Amano, "Influence of the internal structure and temperature in the reaction layer on the electric output in a solar thermal cell," *Enery conversion and management,* pp. 2811-2819, 2003.

[29] P. Chaurasia, Y. Ando and T. Tanaka, "Investigation on proton exchange membrane fuel cell for solar power generation," *International journal of sustainable energy,* pp. 107-119, 2007.

[30] J. Friauf, "Thermodynamics of thermally regenerated fuel cells," *Journal of Applied Physics,* pp. 616-620, 1961.

[31] X. Jin, M. Bishop, T. Ellis and F. Karasz, "A sulphonated poly (aryl ether ketone)," *British Polymer*

Journal, pp. 4-10, 1984.

[32] S. Zaidi, S. Mikhailenko, G. Robertson, M. Guiver and S. Kaliaguine, "Proton conducting composite membranes from polyether ether ketone and heteropolyacids for fuel cell applications," *Journal of Membrane Science,* pp. 17-34, 2000.

[33] R. Huang, P. Shao, C. Burns and X. Feng, "Sulfonation of poly (ether ether ketone)(PEEK): A kinetic study," *Journal of Applied Polymer Science,* pp. 2651-2660, 2001.

[34] S. Kaliaguini, S. Mikhailenko, K. Wang, P. Xing and M. Guiver, "Properties of SPEEK based PEMs for fuel cell applications," *Catalysis Today,* pp. 213-222, 2003.

[35] Q. Li, R. He, J. Jensen and N. Bjerrum, "PBI-Based polymer membranes for high temperature fuel cells - Preparation, characterization and fuel cell demonstration," *Fuel Cells,* pp. 147-159, 2004.

[36] R. Bouchet and E. Siebert, "Proton conduction in acid doping polybenzimidazole," *Solid State Ionics,* vol. 118, pp. 287-299, 1999.

[37] D. Weng, J. Wainwright, U. Landau and R. Savinell, "Electro-osmotic drag coefficient of water and methanol in polymer electrolyte at elevated temperatures," *Journal of the Electrochemical Society,* pp. 1260-1263, 1996.

[38] Y. Ma, J. Wainwright, M. Litt and R. Savinell, "Conductivity of PBI membranes for high-temperature polymer electrolyte fuel cells," *Journal of the Electrochemical Society,* pp. A8-A16, 2004.

[39] Y. Cho, S. Kim, T. Kim, Y. Cho, J. Lim, N. Jung, W. Yoon, J. Lee and Y. Sung, "Preparation of MEA with the polybenzimidazole for high temperature PEM fuel cell," *Electrochemical and Solid-State letters,* pp. B38-B40, 2011.

[40] J. Lobato, P. Canizares, M. Rodrigo, J. Linares and J. Aguilar, "Improved polybenzimidazole films for H3PO4-doped PBI-based high temperature PEMFC," *Journal of Membrane Science,* pp. 47-55, 2007.

[41] J. Zhang, Y. Tang, C. Song and J. Zhang, "Polybenzimidazole-membrane-based PEM fuel cell in the temperature range of 120-200C," *Journal of Power Sources,* vol. 172, pp. 163-171, 2007.

[42] Q. Li, H. Hjuler and N. Bjerrum, "Phosphoric acid doped polybenzimidazole membranes: Physiochemical characterization and fuel cell applications," *Journal of Applied Electrochemistry,* pp. 773-779, 2001.

[43] M. Secanell, K. Karan, A. Suleman and N. Djilali, "Multi-variable optimization of PEMFC cathodes using an agglomerate model," *Electrochimica Acta,* vol. 52, pp. 6318-6337, 2007.

[44] F. Seland, T. Berning, B. Borresen and R. Tunold, "Improving the performance of high-temperature PEM fuel cells based on PBI electrolyte," *Journal of Power Sources,* vol. 160, pp. 27-36, 2006.

[45] O. Kongstein, T. Berning, B. Borresen, F. Seland and R. Tunold, "Polymer electrolyte fuel cells based on phosphoric acid doped polybenzimidazole (PBI) membranes," *Energy,* pp. 418-422, 2007.

[46] Q. Li, H. Rudbeck, A. Chromik, J. Jensen, C. Pan, T. Steenberg, M. Calverly, N. Bjerrum and J. Kerres, "Properties, degradation and high temperature fuel cell test of different types of PBI and PBI blend membranes," *Journal of Membrane Science,* pp. 260-270, 2010.

[47] Y. Oono, A. Sounai and M. Hori, "Influence of the phosphoric acid-doping level in a polybenzimidazole membrane on the cell performance of high-temperature proton exchange membrane fuel cells," *Journal of Power Sources,* vol. 189, pp. 943-949, 2009.

[48] J. Wainwright, J.-T. Wang, D. Weng, R. Savinell and M. Litt, "Acid-doped polybenzimidazoles: a new polymer electrolyte," *Journal of the electrochemical society,* vol. 142, pp. L121-L123, 1995.

[49] J.-T. Wang, J. Wainwright, R. Savinell and M. Litt, "A direct methanol fuel cell using acid-doped polybenzimidazole as polymer electrolyte," *Journal of Applied Electrochemistry,* vol. 26, pp. 751-756, 1995.

[50] Y. Zhai, H. Zhang, G. Liu, J. Hu and B. Yi, "Degradation study on MEA in H3PO4/PBI high-temperature life test," *Journal of the Electrochemical Society,* pp. B72-B76, 2007.

[51] R. O'Hayre, S.-W. Cha, W. Colella and F. Prinz, Fuel cell fundamentals, Hoboken: John Wiley & Sons, 2006.

[52] J. Zuliani, "Summer Internship Final Report," Fuel Cell Research Center (report available at www.fcrc.ca), Kingston, 2012.

[53] Sigma-Aldrich, "Propiophenone," 2012. [Online]. Available: http://www.sigmaaldrich.com/catalog/product/aldrich/w346918?lang=en&region=CA. [Accessed 5 8 2012].

[54] Sigma-Aldrich, "1-phenyl-1-propanol," 2012. [Online]. Available: http://www.sigmaaldrich.com/catalog/product/aldrich/w288403?lang=en&region=CA. [Accessed 5 8 2012].

[55] C. Pan, Q. Li, J. Jensen, R. He, L. Cleemann, M. Nilsson, N. Bjerrum and Q. Zeng, "Preparation and operation of gas diffusion electrodes for high-temperature proton exchange membrane fuel cells," *Journal of Power Sources,* pp. 278-286, 2007.

[56] J. Lobato, P. Canizares, M. Rodrigo, J. Linares and F. Pinar, "Study of the influence of the amount of PBI-H3PO4 in the catalytic layer of high temperature PEMFC," *International Journal of Hydrogen Energy,* pp. 1347-1355, 2010.

[57] T. Soboleva, Z. Xie, Z. Shi, E. Tsang, T. Navessin and S. Holdcroft, "Investigation of the through-plane impedance technique for evaluation of anisotropy of proton conducting polymer membranes," *Journal of Electroanalytical Chemistry,* pp. 145-152, 2008.

[58] C. Marvel and H. Vogel, "Polybenzimidazole; new thermally stable polymers," *Journal of Polymer Science,* vol. L, pp. 511-539, 1961.

[59] Q. Li, R. He, R. Berg, H. Hjuler and N. Bjerrum, "Water uptake and acid doping of polybenzimidazoles as electrolyte membranes for fuel cells," *Solid State Ionics,* vol. 168, pp. 177-185, 2004.

[60] S. Matar, A. Higier and H. Liu, "The effects of excess phosphoric acid in a polybenzimidazole-based high temperature proton exchange membrane based fuel cell," *Journal of Power Sources,* vol. 195, pp. 181-184, 2010.

[61] C. Chen and W. Lai, "Effects of temperature and humidity on the cell performance and resistance of a phosphoric acid doped polybenzimidazole fuel cell," *Journal of Power Sources,* vol. 195, no. 21, pp. 7152-7159, 2010.

[62] T. Schmidt, *Personal correspondance,* 2011.

[63] Sigma-Aldrich, "Phosphoric Acid," 2012. [Online]. Available: http://www.sigmaaldrich.com/catalog/product/SIAL/695017?lang=en&region=CA. [Accessed 10 9 2012].

[64] J. C. Holtz and M. Elliott, "The Significance of Diesel-Exhaust-Gas Analysis," in *Transactions of the ASME*, Pittsburgh, 1941.

[65] N. Espinosa, M. Lazard and L. Aixala, "Modeling a Thermoelectric Generator Applied to Diesel Automotive Heat Recovery," *Journal of Electronic Materials,* pp. 1446-1455, 2010.

[66] R. Werner and R. Shearer, "Fuel Cells". United States Patent 3,031,518, 1962.

[67] T. Doi, Y. Ando, T. Takashima and T. Tanaka, "Study on solar chemical heat pump - basic experiment on falling film reaction of 2-propanol dehydrogenation," in *Energy Conversion Engineering Conference*, Honolulu, 1997.

[68] Q. Li, R. He, J. Jensen and N. Bjerrum, "PBI-based polymer membranes for high temperature fuel cells - preparation, characterization and fuel cell demonstration," *Fuel Cells,* vol. 4, pp. 147-159, 2004.

[69] S. Yu, H. Zhang, L. Xiao, E.-W. Choe and B. Benicewicz, "Synthesis of poly (2,2'-(1,4-phenylene)5,5'-bibenzimidazole)(para-PBI) and phosphoric acid doped membrane for fuel cells," *Fuel Cells,* vol. 09, pp. 318-324, 2009.

Appendix A – Membrane Electrode Assembly Performance and Fabrication Conditions

Table 11: MEAs used in hydrogen-air baseline performance testing

MEA	DL (mol H_3PO_4/repeat unit polymer)	Hot-pressing Pressure (Mpa)	Hot-pressing Temperature (°C)	Hot-pressing Time (minutes)	Gasket Material	Cell Electrical Resistance (Ω)	Reported Fuel Cell Operating Temperature (°C)	Max. Power Density (mW/cm^2)	Current Density at Max. Power Density (mA/cm^2)	Comments
1	9.8	53.4	130	25	Reinforced Silicone	0.272	100	11.1	50	Commercial Pt/C electrodes. Silicone gasket degradation in phosphoric acid at high temperature limited fuel cell operational temperature. Hot pressing pressures far in excess of literature values.
2	3.94	53.4	130	25	Reinforced Silicone	2.14	100	2	10	Commercial Pt/C electrodes. Silicone gasket degradation in phosphoric acid at high temperature limited fuel cell operational temperature. Hot pressing pressures far in excess of literature values.
3	6.21	40.4	130	25	Reinforced Silicone	2.35	100	17.3	60.8	Commercial PBI-impregnated Pt/C electrodes. Silicone gasket degradation in phosphoric acid at high temperature limited fuel cell operational temperature. Hot pressing pressures far in excess of literature values.
4	10.2	68.1	140	25	Reinforced Silicone	0.16	110	212	575	Commercial Pt/C electrodes. High performance attributed to hot-pressing conditions. Silicone gasket degradation in phosphoric acid at high temperature limited fuel cell operational temperature. Hot pressing pressures far in excess of literature values.
5	10.3	54.5	140	25	Reinforced Silicone	0.265	110	118	375	Commercial Pt/C electrodes. High performance attributed to hot-pressing conditions. Silicone gasket degradation in phosphoric acid at high temperature limited fuel cell operational temperature. Hot pressing pressures far in excess of literature values.

MEA	DL (mol H_3PO_4/repeat unit polymer)	Hot-pressing Pressure (Mpa)	Hot-pressing Temperature (°C)	Hot-pressing Time (minutes)	Gasket Material	Cell Electrical Resistance (Ω)	Reported Fuel Cell Operating Temperature (°C)	Max. Power Density (mW/cm^2)	Current Density at Max. Power Density (mA/cm^2)	Comments
6	9.3	90.9	140	25	Reinforced Silicone	0.214	110	187	575	Commercial Pt/C electrodes. High performance attributed to hot-pressing conditions. Silicone gasket degradation in phosphoric acid at high temperature limited fuel cell operational temperature. Hot pressing pressures far in excess of literature values.
7	9.98	54.5	150	25	Reinforced Silicone	not measured	110	189	575	Commercial Pt/C electrodes. High performance attributed to hot-pressing conditions. Silicone gasket degradation in phosphoric acid at high temperature limited fuel cell operational temperature. Hot pressing pressures far in excess of literature values.
8	6.24	16.7	130	25	Reinforced Silicone	0.97	110	118	400	Commercial PBI-impregnated Pt/C electrodes that were subsequently doped with phosphoric acid. Silicone gasket degradation in phosphoric acid at high temperature limited fuel cell operational temperature.
9	6.13	16.7	130	25	Reinforced Silicone	0.387	110	61.5	225	Commercial Pt/C electrodes that were spray-coated in PBI and subsequently doped with phosphoric acid. Silicone gasket degradation in phosphoric acid at high temperature limited fuel cell operational temperature.
10	unknown	N/A	N/A	N/A	Teflon	0.1	160	192	528	Commercial MEA.
11	unknown	N/A	N/A	N/A	Teflon	0.053	160	387	1104	Commercial MEA
12	3.75	50	140	0.33	N/A	N/A	N/A	N/A	N/A	MEA destroyed during hot pressing.
13	4.02	52.3	130	25	Reinforced Silicone	2.35	110	2	12.5	Commercial Pt/C electrodes. Silicone gasket degradation in phosphoric acid at high temperature limited fuel cell operational temperature. Hot pressing pressures far in excess of literature values.

MEA	DL (mol H_3PO_4/repeat unit polymer)	Hot-pressing Pressure (Mpa)	Hot-pressing Temperature (°C)	Hot-pressing Time (minutes)	Gasket Material	Cell Electrical Resistance (Ω)	Reported Fuel Cell Operating Temperature (°C)	Max. Power Density (mW/cm^2)	Current Density at Max. Power Density (mA/cm^2)	Comments
14	9.5	52.3	130	25	Reinforced Silicone	0.339	110	10	55	Commercial Pt/C electrodes. Silicone gasket degradation in phosphoric acid at high temperature limited fuel cell operational temperature. Hot pressing pressures far in excess of literature values.
15	4.92	53.5	130	25	Reinforced Silicone	1.47	110	7.5	40	Commercial Pt/C electrodes. Silicone gasket degradation in phosphoric acid at high temperature limited fuel cell operational temperature. Hot pressing pressures far in excess of literature values.
16	4.98	53.5	130	25	Reinforced Silicone	1.93	100	N/A	N/A	Commercial Pt/C electrodes. Performance degradation at 100C such that polarization curves could not be obtained. Hot pressing pressures far in excess of literature values.
17	7.8	66.8	140	25	N/A	N/A	N/A	N/A	N/A	MEA destroyed during hot pressing.
18	8.22	66.8	140	25	Reinforced Silicone	1.17	110	24	64	Commercial Pt/C electrodes. Silicone gasket degradation in phosphoric acid at high temperature limited fuel cell operational temperature. Hot pressing pressures far in excess of literature values.
19	10.73	66.8	150	25	N/A	N/A	N/A	N/A	N/A	MEA destroyed during hot pressing.
20	6.02	40.4	130	25	Reinforced Silicone	2.47	100	94	182	Commercial PBI-impregnated Pt/C electrodes. Same DL, assembly conditions and cell temperature as MEA#3, but tested at 30 kPag backpressure and not readily comparable. Silicone gasket degradation in phosphoric acid at high temperature limited fuel cell operational temperature. Hot pressing pressures far in excess of literature values.
21	5.32	122.6	130	25	Reinforced Silicone	5.23	110	15	50	Commercial PBI-impregnated Pt/C electrodes. Silicone gasket degradation in phosphoric acid at high temperature limited fuel cell operational temperature.

MEA	DL (mol H_3PO_4/repeat unit polymer)	Hot-pressing Pressure (Mpa)	Hot-pressing Temperature (°C)	Hot-pressing Time (minutes)	Gasket Material	Cell Electrical Resistance (Ω)	Reported Fuel Cell Operating Temperature (°C)	Max. Power Density (mW/cm^2)	Current Density at Max. Power Density (mA/cm^2)	Comments
22	5.5	171.6	140	25	Reinforced Silicone	6.3	N/A	N/A	N/A	Could not be assembled without crossover leak detection.
23	5.31	94.6	130	25	Reinforced Silicone	4.57	N/A	N/A	N/A	Could not be assembled without crossover leak detection.
24	6.13	94.6	130	25	N/A	N/A	N/A	N/A	N/A	MEA destroyed during hot pressing.
25	7.63	15	130	25	Teflon	0.38	N/A	N/A	N/A	Commercial acid-doped PBI-impregnated Pt/C electrodes. Could not be tested because OCV did not ever stabilize, but dropped below 0.3V.
26	unknown	N/A	N/A	N/A	Teflon	not measured	160	296	740	Commercial MEA. Air and Hydrogen flowrates in between those of MEA#10/#11. Instability noted during testing at temperatures over 110°C and reported performance is not necessarily steady state; explanation unknown. Silicone gasket degradation in phosphoric acid at high temperature limited fuel cell operational temperature.
27	unknown	N/A	N/A	N/A	Teflon	0.063	110	76	253	Commercial MEA. Cell possibly contaminated with propiophenone from an earlier trial. Silicone gasket degradation in phosphoric acid at high temperature limited fuel cell operational temperature.
28	unknown	N/A	N/A	N/A	Teflon	0.053	160	366	1200	Commercial MEA.

Table 12: MEAs used in TRFC performance testing

MEA	DL (mol H_3PO_4/repeat unit polymer)	Hot-pressing Pressure (Mpa)	Hot-pressing Temperature (°C)	Hot-pressing Time (minutes)	Gasket Material	Cell Electrical Resistance (Ω)	Reported Fuel Cell Operating Temperature (°C)	Max. Power Density (mW/cm^2)	Current Density at Max. Power Density (mA/cm^2)	Comments
11	unknown	N/A	N/A	N/A	Teflon	0.053	160	0.0402	1.3	Commercial MEA.
12	unknown	N/A	N/A	N/A	Teflon	0.058	160	0.0296	0.84	Commercial MEA.

Appendix B – Sample Calculations

TRFC Current Draw – at maximum power density of MEA#111under TRFC operation at 160°C

$$Current = \frac{voltage}{resistance}$$

$$= \frac{0.031\,V}{2.7\,\Omega}$$

$$= 0.011\,A$$

Current Density – at maximum power density of MEA#28 under hydrogen-air operation at 160°C

$$Current\ density = \frac{current\ draw}{electrode\ active\ area}$$

$$= \frac{10.74\,A}{8.8\,cm^2}$$

$$= 1.22\ \frac{A}{cm^2}$$

Power Density – at maximum power density of MEA#28 under hydrogen-air operation at 160°C

$$Power\ density = current\ density * voltage$$

$$= 1.22\ \frac{A}{cm^2} * 0.3\,V$$

$$= 0.366\ \frac{W}{cm^2}$$

In-plane Membrane Conductivity – using the values in Table 10 for PBI membrane with DL 2.81 immersed in propiophenone at 140°C

$$In - plane\ conductivity\ (\sigma)$$

$$= \frac{membrane\ length}{membrane\ width * membrane\ thickness * measured\ resistance}$$

$$= \frac{2{,}4\ cm}{2.4\ cm * 0.004\ cm * 1277.5\ \Omega}$$

$$= 0.204\ \frac{S}{cm}$$

(Note that this value is not the same as the one reported in the body of this work (0.181 S/cm^2). Here it has been assumed that the membrane width was 2.4 cm, but evidently this was not the case in the actual experiment.)

Total Equivalents - calculated for the final 2 seconds of the 16 hour TRFC operation described in the body of this work

$$Total\ equivalents = \frac{measured\ current\ at\ t_i * \Delta t}{Faraday's\ constant} + \sum_{t_0}^{t_{i-1}} Equilavents$$

$$= \frac{0.00323\ A * 2\ s}{96485.3\ \frac{C}{mol}} + \ 0.00293\ equivalents$$

$$= 0.00293\ equivalents$$

Membrane Doping Level – calculated for MEA#1

$$Doping\ level = \frac{mols\ phosphoric\ acid\ in\ membrane}{repeat\ units\ of\ polymer\ in\ membrane}$$

$$Mols\ phosphoric\ acid\ in\ membrane$$

$$= \frac{(membrane\ weight\ after\ doping -\ membrane\ weight\ before\ doping)}{molecular\ weight\ of\ phosphoric\ acid}$$

$$= \frac{0.2047g - 0.0499g}{98\ \frac{g}{mol}}$$

$$= 1.6x10^{-3} mol\ phosphoric\ acid$$

$$Repeat\ units\ of\ polymer\ in\ membrane = \frac{membrane\ weight\ before\ doping}{molecular\ weight\ of\ polymer\ repeat\ unit}$$

$$= \frac{0.0499g}{310 \frac{g}{mols\ repeat\ unit\ PBI}}$$

$$= 1.61x10^{-4}\ mol\ repeat\ unit\ PBI$$

$$Doping\ level = \frac{1.6x10^{-3} mol\ phosphoric\ acid}{1.61x10^{-4}\ mol\ repeat\ unit\ PBI}$$

$$= 9.94\ \frac{mol\ phosphoric\ acid}{mol\ repeat\ unit\ PBI}$$

<u>ΔH from van’t Hoff plot</u>

$$van't\ Hoff\ equation{:} \ln K = -\frac{\Delta H}{RT} + \frac{\Delta S}{R}$$

$$\Delta H = -slope * R$$

$$= -6688.5\ ℃ * 8.314 \frac{J}{mol\ K}$$

$$= -55.6\ \frac{kJ}{mol}$$

<u>ΔS from van't Hoff plot</u>

$$\Delta S = y - intercept * R$$

$$= -14.1 * 8.314\ \frac{J}{mol\ K}$$

$$= -117.2\ \frac{J}{mol\ K}$$

<u>Cell Potential from Gibb's Free Energy</u> – calculated for hydrogenation of propiophenone at 160°C using data from Table 3.

$$E^{\circ}_{cell} = \frac{\Delta G^{\circ}}{-nF}$$

$$= -\frac{-4900\ \frac{J}{mol}}{2\ * 96485\ \frac{C}{mol}}$$

$$= 0.025\ V = 25\ mV$$

Appendix C – Hot Pressing Procedure

The hot-pressing error described in this work was due to an incorrect assumption of the area over which pressure was distributed. It was assumed that pressure would be distributed across the entire hot-pressing plate area because of the relatively low thickness of the membrane and electrodes.

Later studies showed that in fact the pressure was distributed only across the electrode area. This error led to overpressing of MEAs by a factor of approximately 30. A procedure for the correct method of hot-pressing is presented below.

$$Electrode\ active\ area = 4\ cm^2$$

$$Desired\ hot\ pressing\ pressure = 15\ MPa = 153\ \frac{kg}{cm^2}$$

$$Required\ force = Electrode\ active\ area * Desired\ hot\ pressing\ pressure$$

$$= 4\ cm^2 * 153\ \frac{kg}{cm^2}$$

$$Required\ force = 612\ kg\ (as\ per\ the\ indicator\ on\ the\ press)$$

Appendix D - Safety Considerations

Chemical Hazards

The chemicals used in this experimental work are not carcinogenic, however certain precautions were taken. Propiophenone is an irritant with an LD_{50} value for mice of 4.5 g/kg [53]. 1-phenyl-1-propanol is a central nervous system depressant which if inhaled in high quantities can lead to pulmonary edema [54]. 1-phenyl-1-propanol has a reported LD_{50} for mice of 0.5 g/kg. Ventilation is advised when working with both substances.

Both propiophenone and 1-phenyl-1-propanol are combustible liquids and should be kept out of contact with any potential sources of ignition.

Phosphoric acid is corrosive, especially at high concentrations [63]. Acid should never come into contact with bare skin and any contaminated clothing should be removed immediately.

If any chemicals come into contact with eyes or skin the affected area should be rinsed with distilled water for 10 minutes.

Physical Hazards

Working with fuel cells presents both temperature and electricity-related dangers. Heat-proof gloves must be worn when working with materials at high temperature, and care should be taken to never contact an electrified object.